© 2021. Published by The Company of Biologists Ltd | Development (2021) 148, dev199549. doi:10.1242/dev.199549

RESEARCH ARTICLE

Multiple PDZ domain protein maintains patterning of the apical cytoskeleton in sensory hair cells

Amandine Jarysta[1] and Basile Tarchini[1,2,3,*]

ABSTRACT

Sound transduction occurs in the hair bundle, the apical compartment of sensory hair cells in the inner ear. The hair bundle is formed of actin-based stereocilia aligned in rows of graded heights. It was previously shown that the GNAI-GPSM2 complex is part of a developmental blueprint that defines the polarized organization of the apical cytoskeleton in hair cells, including stereocilia distribution and elongation. Here, we report a role for multiple PDZ domain (MPDZ) protein during apical hair cell morphogenesis in mouse. We show that MPDZ is enriched at the hair cell apical membrane along with MAGUK p55 subfamily member 5 (MPP5/PALS1) and the Crumbs protein CRB3. MPDZ is required there to maintain the proper segregation of apical blueprint proteins, including GNAI-GPSM2. Loss of the blueprint coincides with misaligned stereocilia placement in *Mpdz* mutant hair cells, and results in permanently misshapen hair bundles. Graded molecular and structural defects along the cochlea can explain the profile of hearing loss in *Mpdz* mutants, where deficits are most severe at high frequencies.

KEY WORDS: Cell polarity, Cytoskeleton, Inner ear, Morphogenesis, Mouse genetics, Sensory hair cell, Mouse

INTRODUCTION

Auditory function relies on the ability of sensory hair cells (HCs) in the auditory epithelium to detect sound vibrations. Detecting mechanical vibrations is the role of the hair bundle, a highly organized brush of actin-based membrane protrusions, or stereocilia, located at the HC apical surface. Mutations affecting proteins involved in the morphogenesis or the maintenance of the hair bundle lead to hearing loss (Barr-Gillespie, 2015; McGrath et al., 2017; Petit and Richardson, 2009; Velez-Ortega and Frolenkov, 2019).

We and others showed that inhibitory guanine nucleotide-binding proteins (G proteins) of the alpha family (GNAI1-3, collectively GNAI) bind the scaffold protein G protein signaling modulator 2 (GPSM2) to form a complex essential for the polarized morphogenesis of the apical cytoskeleton in HCs (Beer-Hammer et al., 2018; Bhonker et al., 2016; Ezan et al., 2013; Mauriac et al., 2017; Tadenev et al., 2019; Tarchini et al., 2013, 2016). Post-mitotic HCs are initially covered uniformly with microvilli, but planar-polarized enrichment of GNAI-GPSM2 and inscuteable (INSC) at the apical membrane defines a lateral/abneural region without protrusions, termed the bare zone (Tarchini et al., 2013). GNAI-GPSM2 generates and expands the bare zone by antagonizing the polarity kinase aPKC present on the HC surface decorated with microvilli. Complementary GNAI-GPSM2 and aPKC distribution thus forms an apical blueprint that defines the lateral edge of the emerging hair bundle when microvilli grow into stereocilia (Tarchini et al., 2013). As HCs mature, the GNAI-GPSM2 complex is then trafficked to the tips of stereocilia adjacent to the bare zone by the MYO15A motor (Mauriac et al., 2017; Tadenev et al., 2019; Tarchini et al., 2016). At stereocilia tips, GNAI-GPSM2 promotes enrichment of MYO15A and other partners, conferring the first stereocilia row with its characteristic tallest height (Tadenev et al., 2019). Loss of GNAI or GPSM2 in mouse leads to stunting of stereocilia, and the resulting immature hair bundle morphology in adults coincides with profound deafness (Beer-Hammer et al., 2018; Mauriac et al., 2017; Tarchini et al., 2016). In humans, mutations in *GPSM2* are responsible for the Chudley–McCullough syndrome in which hearing loss is the principal affliction (Doherty et al., 2012; Walsh et al., 2010).

GNAI-GPSM2 is enriched and polarized independently of core planar cell polarity (PCP) proteins (Ezan et al., 2013; Tarchini et al., 2013), the machinery that regulates HC orientation via intercellular communication at apical cell-cell junctions (Deans, 2013; Tarchini and Lu, 2019). Accordingly, polarization of a subset of core PCP proteins was recently proposed to depend on Wnt secretion, but severely disrupted cochlear elongation and morphogenesis in *Wntless* (*Wls*) mutants left GNAI-GPSM2 enrichment intact at the HC surface (Landin Malt et al., 2020; Najarro et al., 2020). Similarly, polarized segregation of GNAI-GPSM2 and aPKC was preserved in mutants lacking other polarity proteins that occupy the lateral apical HC junction: DAPLE (CCDC88C) (Siletti et al., 2017) and PARD3 (Landin Malt et al., 2019). It thus remains unclear how GNAI-GPSM2 is first polarized and then maintained at the HC apical membrane. Here, we hypothesized that GNAI-GPSM2 might interact more specifically with polarity proteins that occupy the HC apical membrane. To find possible candidates, we investigated proteins that are known to establish apico-basal polarization in other epithelial systems.

Multiple PDZ domain (MPDZ, or MUPP1) is a large adapter protein with 13 PDZ (PSD95/DLG1/ZO1) domains that mediates protein-protein interactions and was first reported to interact with the HTR2C serotonin receptor (Simpson et al., 1999; Ullmer et al., 1998). MPDZ is a scaffold protein that clusters binding partners in defined cell compartments, for example SynGAP and CaMKII at synapses (Krapivinsky et al., 2004), as well as delta like protein 1 and 4 (DLL1/4) and NECTIN2 at epithelial apical junctions (Tetzlaff et al., 2018). MPDZ is a paralog of INADL/PATJ, a scaffolding protein that binds MPP5 (PALS1), with MPP5 in turn binding the integral protein CRB3 to form the Crumbs complex (Lemmers et al., 2002; Makarova et al., 2003; Roh et al., 2003,

[1]The Jackson Laboratory, Bar Harbor, ME 04609, USA. [2]Department of Medicine, Tufts University, Boston, MA 02111, USA. [3]Graduate School of Biomedical Science and Engineering (GSBSE), University of Maine, Orono, ME 04469, USA.

*Author for correspondence (basile.tarchini@jax.org)

A.J., 0000-0002-9519-3559; B.T., 0000-0003-2708-6273

Handling Editor: Thomas Lecuit
Received 20 February 2021; Accepted 25 June 2021

Development (2021) 148, dev199549. doi:10.1242/dev.199549

2002). The Crumbs complex plays a highly conserved role in the establishment of epithelial apico-basal polarity (Assémat et al., 2008; Tepass, 2012), including the formation of tight junctions in mammals (Charrier et al., 2015; Hurd et al., 2003; Roh et al., 2003, 2002; Shin et al., 2005; Whiteman et al., 2014). MPDZ itself was reported to be a component of tight junctions, and MPDZ can directly bind claudins (Hamazaki et al., 2002; Lanaspa et al., 2008; Poliak et al., 2002) as well as many of the INADL partners, including JAM1 (F11R) (Adachi et al., 2009; Hamazaki et al., 2002) and ZO1 (TJP1) (Adachi et al., 2009). Interestingly, like INADL, MPDZ can bind MPP5 to form an alternative Crumbs complex (CRB3-MPP5-MPDZ) with cellular functions that are distinct from the better-described CRB3-MPP5-INADL complex (Adachi et al., 2009; Roh et al., 2002). Recently, MPDZ was shown to bind and cooperate with DAPLE at apical junctions to elicit apical cell constriction in cell culture and during neurulation (Marivin and Garcia-Marcos, 2019; Marivin et al., 2019).

In humans and mice, mutations in *MPDZ* lead to multiple ependymal malformations that compromise the lining of the brain ventricles (Feldner et al., 2017; Saugier-Veber et al., 2017). These defects were initially proposed to result from defective ependymal tight junctions, but a recent study also uncovered a more specific role for MPDZ in the choroid plexus, which secretes cerebrospinal fluid into the ventricles (Yang et al., 2019). Interestingly, although barrier integrity was defective in both organs, MPDZ has to date only been reported apically in choroid plexus epithelial cells, and was not visibly enriched at tight junctions there (Yang et al., 2019). *MPDZ* is one of the few genes linked to congenital hydrocephalus in humans (Al-Dosari et al., 2013; Al-Jezawi et al., 2018; Saugier-Veber et al., 2017; Shaheen et al., 2017) and mice (Feldner et al., 2017; Yang et al., 2019), likely as a result of ependymal and/or choroid plexus dysfunction when mutated. Of note, a young patient carrying two distinct *MPDZ* mutations in *trans* also presented with sensorineural hearing loss, suggesting a potential role for MPDZ in the inner ear (Shaheen et al., 2017).

In this study, we identify a new function for MPDZ during HC development. Surprisingly, MPDZ is not detected at apical cell junctions in the auditory epithelium, but at the HC apical membrane where it colocalizes with MPP5 and CRB3. We show that MPDZ is necessary to maintain the apical segregation of GNAI-GPSM2 and aPKC. Loss of this apical blueprint in *Mpdz* mutants coincides with misaligned stereocilia placement and dysmorphic hair bundles. Molecular and morphological defects persist in young adults and are likely responsible for severe hearing loss in *Mpdz* mutants.

RESULTS

MPDZ occupies the hair cell apical membrane with a lateral bias

To investigate a potential role for MPDZ in the auditory epithelium, we started by immunolabeling MPDZ at different developmental stages with a validated antibody targeting the third PDZ domain (PDZ3) (Poliak et al., 2002). As early as embryonic day (E) 17.5, MPDZ signal was obvious at the HC apex, spanning most of the apical membrane (Fig. 1A). MPDZ was most highly enriched at the bare zone, the flat region deprived of protrusions lying lateral to the tallest stereocilia (Tarchini et al., 2013). MPDZ signal was lower on the medial side of the hair bundle, and absent or barely detectable at the position of the hair bundle itself. A similar MPDZ enrichment pattern was observed in neonate HCs at postnatal day (P) 0 and P4 (Fig. 1A). Of note, INSC, GNAI and GPSM2 are, by contrast, strictly enriched at the bare zone and are thus more obviously planar polarized than MPDZ (Bhonker et al., 2016; Ezan et al., 2013; Tarchini et al., 2013). MPDZ was limited to the HC apical membrane (Fig. 1B), and no enrichment was detected at apical HC junctions labeled with ZO1 (Fig. 1B).

Loss of MPDZ results in apical defects in developing hair cells

We obtained a constitutive *Mpdz* mouse mutant from the Knockout Mouse Project (KOMP) (C57BL/6N-*Mpdz*$^{em1(IMPC)J}$/Mmucd, hereafter *Mpdz*^{DEL}). This strain carries an indel in *Mpdz* exon 6, which is predicted to cause a frameshift resulting in early truncation of the protein after the first of 13 PDZ domains. We did not observe lethality in *Mpdz*$^{DEL/DEL}$ animals, whereas previous *Mpdz* mutants died at around 3-4 weeks of age (Feldner et al., 2017; Milner et al., 2015; Yang et al., 2019). Nevertheless, as expected, MPDZ antibody signal was not observed in the *Mpdz*$^{DEL/DEL}$ auditory epithelium (Fig. 1A). Signal was also absent in choroid plexus epithelial cells where MPDZ was previously reported with the same antibody (Fig. S1A) (Yang et al., 2019), establishing *Mpdz*^{DEL} as a suitable loss-of-function model (see Discussion and Table S1 for a summary of the differences between mouse strains).

Based on its localization, we investigated whether MPDZ could be involved in apical HC morphogenesis. We first imaged the hair bundle at embryonic and postnatal stages using conjugated phalloidin to reveal F-actin. At E17.5, stereocilia organization appeared comparable between *Mpdz* mutants and littermate controls at the cochlear base (Fig. 1C). However, by birth (P0), and at P4, apical HC defects were obvious in outer HCs (OHCs), where hair bundles lacked their characteristic V-shape and were frequently split (Fig. 1C). Because three-dimensional organization of protruding stereocilia can be confusing in flat-mounts, we labeled stereocilia rootlets at P6 with an antibody against TRIOBP (Katsuno et al., 2019). We found that stereocilia placement was severely misaligned in *Mpdz* mutants (Fig. 1D). Stereocilia also formed incomplete supernumerary rows that were most obvious on the lateral side of the bundle at P6 (Fig. 1D, arrowheads). Inner HCs (IHCs) showed similar, but milder defects from P0 (Fig. 1C,D). Defective hair bundles could still take up the styryl dye FM 1-43 in P4 *Mpdz* mutants, an indication of grossly normal mechanosensory channel function (Fig. S1B). Together, these results suggest that MPDZ acts at the apical membrane outside of the forming hair bundle and is important for the proper localization and cohesive, arrayed organization of stereocilia in postnatal HCs.

Labeling of apical junctions with ZO1 revealed abnormally round HC circumference in P4 *Mpdz* mutants compared with control littermates (Fig. 1E). We quantified the apical surface area in HCs and observed a significant reduction in *Mpdz* mutants at the cochlear base and apex at P4, but not at P0 (Fig. 1F). The HC apical surface is known to decrease after P0 along with a remodeling of the cell circumference that closely mirrors hair bundle development, and transitions from circular to peanut-shaped (Etournay et al., 2010). We next quantified the circularity of the HC apical domain. At P4, OHCs in *Mpdz* mutants maintained a rounder shape (higher circularity) compared with control littermates, but no significant difference was seen at P0 (Fig. 1G). IHCs in *Mpdz* mutants showed a slight decrease of circularity at P0, but not at P4. MPDZ might thus regulate HC apical surface remodeling, impacting both the placement of stereocilia and the shape of the HC junctions. GNAI and GPSM2 share MPDZ localization at the bare zone, and are also essential to define the lateral outline of the forming hair bundle

Development (2021) 148, dev199549. doi:10.1242/dev.199549

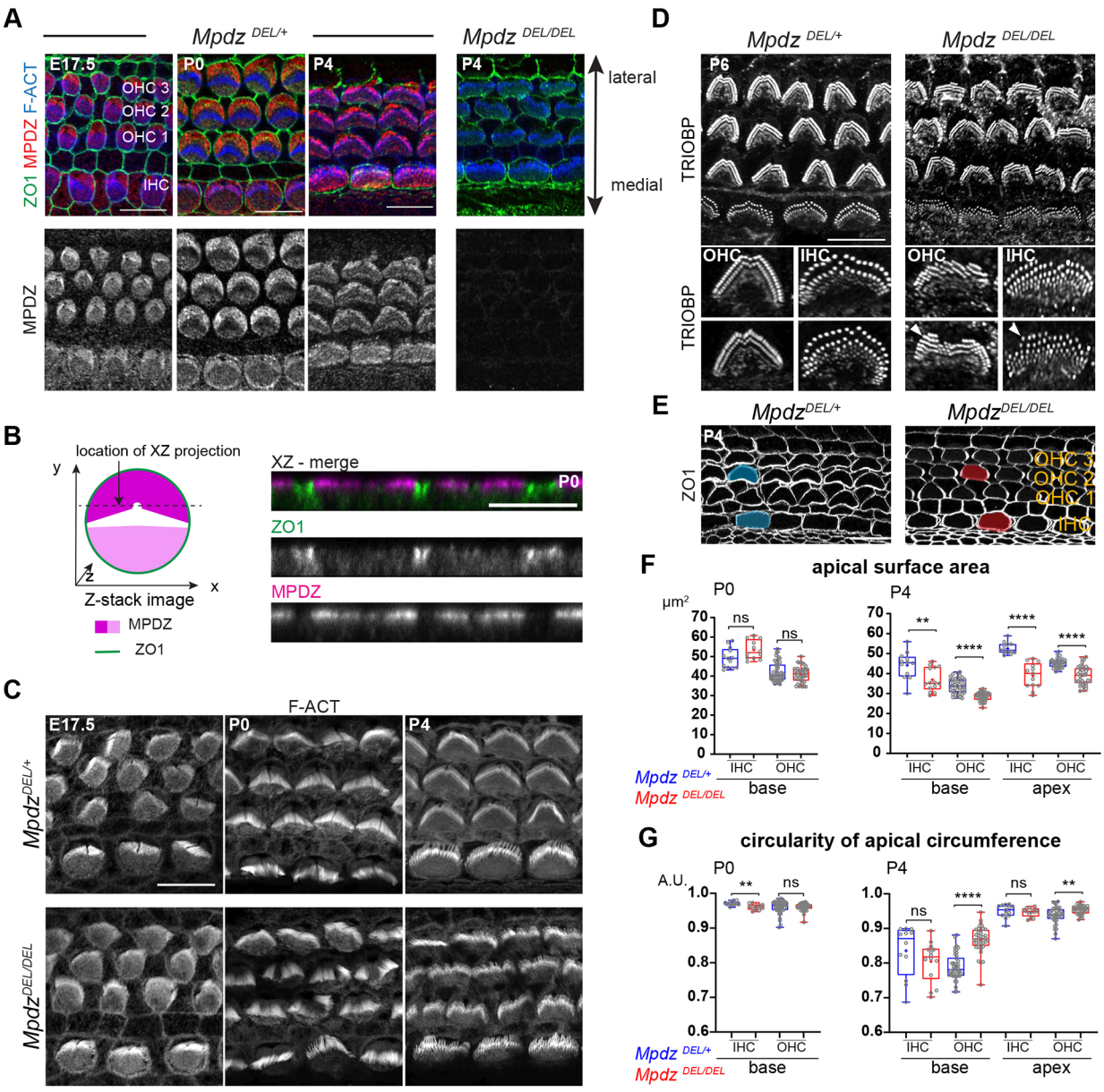

Fig. 1. MPDZ occupies the hair cell apical membrane and is required for normal stereocilia distribution and apical junction circumference in neonates. (A) Flat-mount views of the mouse auditory epithelium immunolabeled with MPDZ (red), ZO1 (green, apical junctions) and phalloidin (blue, F-actin) at E17.5, P0 and P4 (cochlear base). MPDZ signal is entirely lost in *Mpdz* mutants ($Mpdz^{DEL/DEL}$). (B) Projection (*xz*) view of the immunolabeled auditory epithelium at P0 as illustrated in the schematic on the left (high MPDZ enrichment at the bare zone shown in dark magenta; lower enrichment at the medial domain, light magenta). MPDZ is detected at the HC apical membrane, but not at junctions labeled with ZO1. (C) Phalloidin (F-actin) labeling of the hair bundle (cochlear base; maximal projection). In the absence of MPDZ, OHC and IHC hair bundles are misshapen from P0. (D) TRIOBP labeling of the stereocilia rootlets at P6 (maximal projection). Stereocilia are misaligned and form interrupted or supernumerary rows (arrowheads) in *Mpdz* mutants. (E) ZO1 labeling of the apical junctions at P4 (cochlear base). In the absence of MPDZ, the HC circumference is abnormally rounded, and the apical surface appears reduced (apical surface shaded in blue in $Mpdz^{DEL/+}$, red in $Mpdz^{DEL/DEL}$ in a single HC). (F) Apical surface area at P0 and P4 based on ZO1 labeling. Here, and in the following figures, graphical representations show a 25-75% percentile box plot in which external bars show the minimum and maximum, the internal bar shows the median and the cross shows the mean. All individual data points are also shown. P0 base: $Mpdz^{DEL/+}$ *N*=3 animals, *n*=13 IHC, *n*=45 OHC; $Mpdz^{DEL/DEL}$ *N*=3, *n*=13 IHC, *n*=40 OHC. P4 base: $Mpdz^{DEL/+}$ *N*=3, *n*=12 IHC, *n*=42 OHC; $Mpdz^{DEL/DEL}$ *N*=3, *n*=14 IHC, *n*=38 OHC. P4 apex: $Mpdz^{DEL/+}$ *N*=3, *n*=13 IHC, *n*=36 OHC; $Mpdz^{DEL/DEL}$ *N*=3, *n*=13 IHC, *n*=35 OHC (Mann–Whitney *U*-test; P0: IHC P=0.0523, OHC P=0.4417; P4 base: IHC $^{**}P$=0.0054, OHC $^{****}P$<0.0001; P4 apex: IHC $^{****}P$<0.0001, OHC $^{****}P$<0.0001; ns, not significant). (G) Circularity of the HC apical circumference based on ZO1 labeling. Animal (*N*) and cell (*n*) numbers are the same as in F (Mann–Whitney *U*-test; P0: IHC $^{**}P$=0.0025, OHC P=0.3513; P4 base: IHC P=0.1274, OHC $^{****}P$<0.0001; P4 apex: IHC P=0.3825, OHC $^{**}P$=0.0023; ns, not significant). Scale bars: 10 µm (A,C-E); 5 µm (B).

(Bhonker et al., 2016; Ezan et al., 2013; Tarchini et al., 2013), as well as the asymmetry of height and identities across stereocilia rows (Mauriac et al., 2017; Tadenev et al., 2019; Tarchini et al., 2016). Next, we thus analyzed the localization of GNAI-GPSM2 in *Mpdz* mutants.

Loss of MPDZ causes a progressive delocalization of GNAI-GPSM2 at the hair cell surface

We assessed GNAI localization in HCs in the first postnatal week. At P0 or P2 (Fig. 2A), GNAI was distributed normally in *Mpdz* mutant HCs along the whole cochlea. In contrast, at P4 many OHCs

Development (2021) 148, dev199549. doi:10.1242/dev.199549

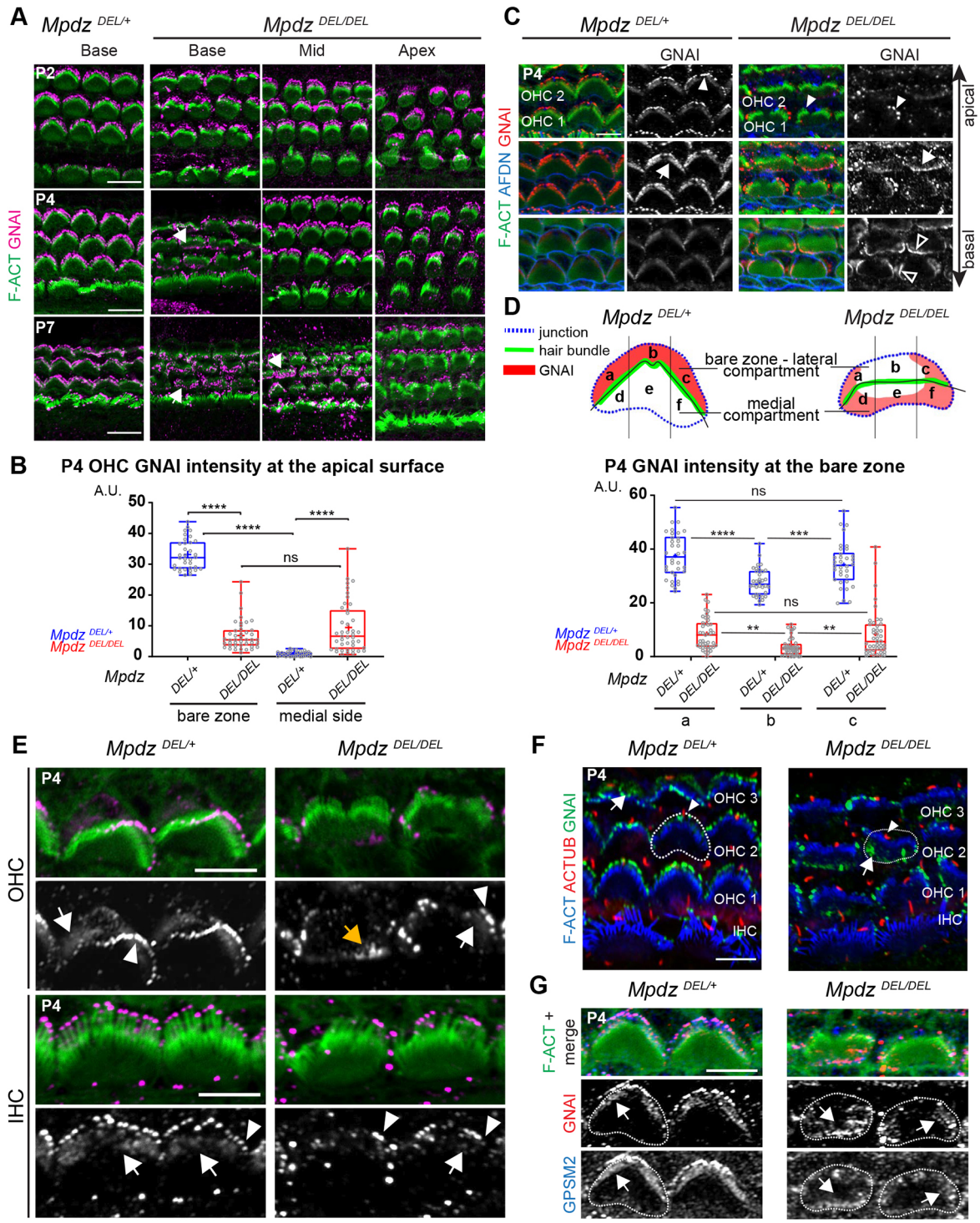

Fig. 2. See next page for legend.

at the cochlear base showed medial delocalization of GNAI, whereas HCs at mid and apex cochlear positions retained normal GNAI distribution. At P7, all OHCs at the base and many OHCs at the mid position showed delocalized GNAI, and HCs at the apex retained normal GNAI distribution. We conclude that loss of MPDZ progressively alters apical GNAI distribution as HC differentiation progresses temporally and spatially along a cochlear apex-to-base gradient (McKenzie et al., 2004). Quantification of GNAI signal intensity in P4 OHCs confirmed a drastic delocalization from the lateral to the medial side of the hair bundle. Compared with control littermates, GNAI enrichment at the lateral bare zone decreased, and medial GNAI enrichment increased in *Mpdz* mutants (Fig. 2B).

We next attempted to define more precisely how GNAI was redistributed in *Mpdz* mutant HCs. In P4 mutant OHCs at the cochlear base, GNAI was variably depleted at the center of the bare zone and at stereocilia tips, but was generally retained at the bare zone periphery (Fig. 2C). Interestingly, GNAI was ectopically

Development (2021) 148, dev199549. doi:10.1242/dev.199549

Fig. 2. Apical enrichment of GNAI and GPSM2 is progressively reduced and delocalized in the absence of MPDZ. (A) GNAI immunolabeling (magenta) at different postnatal stages and positions along the cochlea (maximal projection). In *Mpdz* mutants, GNAI enrichment at the lateral bare zone and in neighboring stereocilia is compromised at the cochlear base at P4 (arrows), and this defect extends to the cochlear mid by P7. (B) GNAI enrichment at the lateral (bare zone) and medial apical surface in P4 OHCs. $Mpdz^{DEL/+}$ *N*=3 animals, *n*=34 OHC; $Mpdz^{DEL/DEL}$ *N*=3, *n*=43 OHC (Kruskal–Wallis with Dunn's multiple comparison test; bare zone versus medial side: $Mpdz^{DEL/+}$, ****P<0.0001, $Mpdz^{DEL/DEL}$, P>0.9999; $Mpdz^{DEL/+}$ versus $Mpdz^{DEL/DEL}$: bare zone and medial side, ****P<0.0001). (C) GNAI labeling at P4 at three different apico-basal *z* levels of the same confocal stack (OHC1-2 field at the cochlear base). F-actin labels stereocilia and afadin (AFDN) labels the apical junctions. In *Mpdz* mutants, GNAI enrichment is generally reduced, and often delocalized medially at the flat HC apex (arrows) and partially lost in the stereocilia (filled arrowheads). GNAI is also ectopically detected at medial apical junctions below the flat apex (unfilled arrowheads). (D) GNAI enrichment across the bare zone in P4 OHCs. The schematic depicts GNAI enrichment compared with the HC junction and the hair bundle in control and *Mpdz* mutant. The OHCs apical surface was divided into three sub-regions of equal width (a, b, c) and GNAI signal was measured by sub-region. $Mpdz^{DEL/+}$ *N*=3, *n*=34 OHC; $Mpdz^{DEL/DEL}$ *N*=3, *n*=43 OHC. Two-way ANOVA with Sidak's multiple comparison test ($Mpdz^{DEL/+}$: a versus b ****P<0.0001; b versus c ***P=0.0003; a versus c P=0.1503; $Mpdz^{DEL/DEL}$: a versus b **P=0.0025; b versus c **P=0.0042; a versus c P=0.9984). (E) GNAI enrichment at higher magnification in two representative P4 OHCs and IHCs (cochlear base; maximal projection). Note how in *Mpdz* mutant HCs, GNAI signal is reduced, particularly at the flat HC apex. In OHCs, GNAI is only retained in a subset of peripheral stereocilia (arrowheads) adjacent to where GNAI is retained at the peripheral region of the bare zone (white arrows). Alternatively, GNAI is delocalized medially at the HC flat surface (orange arrow) and missing in the hair bundle entirely. (F) Co-immunolabeling of GNAI (green) and acetylated tubulin (ACTUB, red) to reveal the kinocilium at P4 (cochlear base; maximal projection). As in control HCs, the kinocilium (arrowheads) is localized lateral to the hair bundle in *Mpdz* mutant OHCs, even when GNAI is delocalized medially (arrows). (G) GNAI-GPSM2 co-labeling in P4 OHCs (cochlear base). Delocalized GNAI and GPSM2 (arrows) still colocalize in *Mpdz* mutants. In F and G, select HC circumferences are outlined. A.U., arbitrary units. Scale bars: 10 µm (A); 5 µm (C,E-G).

found (1) at the medial apical membrane (Fig. 2C, arrow), and (2) at the medial HC junction with the neighboring support cell labeled with afadin (AFDN) (Fig. 2C, unfilled arrowheads). We quantified this trend by measuring GNAI enrichment in three equal subregions of the bare zone along the longitudinal axis (Fig. 2D; regions a, b, c). GNAI signal was ∼20% lower in the central subregion (b) compared with the peripheral subregions (a, c) in control animals, likely reflecting the absence of GNAI near the basal body. In contrast, GNAI signal was ∼60% lower in the central subregion (b) compared with the peripheral subregions (a, c) in *Mpdz* mutants. We also quantified GNAI enrichment in three equal subregions on the medial side of the hair bundle (Fig. S2). Ectopic GNAI signal appeared to be equivalent in the three medial subregions in *Mpdz* mutants. These results suggest that GNAI restriction to the bare zone is first compromised centrally near the basal body starting at P4, and that GNAI progressively invades the medial apical membrane, perhaps relocalizing from the lateral to the medial side.

Interestingly, GNAI presence or absence at stereocilia tips coincided spatially with GNAI presence or absence at the adjacent portion of the bare zone in single OHCs (Fig. 2E). When GNAI was only maintained at the bare zone periphery (Fig. 2E, white arrows), GNAI was only maintained at the tips of peripheral stereocilia in the hair bundle (Fig. 2E, white arrowheads). Complete medial relocalization of GNAI outside the hair bundle (Fig. 2E, orange arrow) was paired with an almost complete loss of GNAI at tips. GNAI-GPSM2 enrichment at the bare zone is progressively reduced during HC maturation (Tarchini et al., 2013). Low amounts of GNAI at the bare zone in P4 IHCs made delocalization to the flat surface and pairing with outcomes at tips challenging to assess. We did, however, observe reduced GNAI bare zone enrichment in *Mpdz* mutant IHCs compared with controls, and a similar but less severe loss of GNAI at stereocilia tips compared with OHCs (Fig. 2E). Spatial pairing of GNAI between HC compartments in *Mpdz* mutants supports our working model whereby prior GNAI-GPSM2 enrichment at the bare zone instructs its selective trafficking to adjacent stereocilia in the first row (Tadenev et al., 2019; Tarchini et al., 2016).

Because disrupted hair bundle morphology obscured hair bundle orientation in *Mpdz* mutants, we next immunolabeled the kinocilium at P4. As in control HCs, the kinocilium was systematically located on the lateral side of the hair bundle in *Mpdz* mutants (Fig. 2F, arrowheads). This clarifies that the progressive delocalization of GNAI to the medial apex does not reflect a change in HC orientation. As expected, the GNAI binding partner GPSM2 also delocalized in a similar manner to GNAI in *Mpdz* mutants (Fig. 2G).

The hair cell apical blueprint is globally disrupted in the absence of MPDZ

INSC-GNAI-GPSM2 at the bare zone antagonizes aPKC at the medial apical surface, and the boundary between these two apical membrane compartments coincides with the lateral edge of the forming hair bundle (Bhonker et al., 2016; Ezan et al., 2013; Tarchini et al., 2013). Similar to GNAI and GPSM2, aPKC lost its spatial restriction in *Mpdz* mutants. At the cochlear base at P4, aPKC was restricted to the medial HC apex in control OHCs and IHCs, but found ectopically across the whole apical surface in *Mpdz* mutants (Fig. 3A). Measuring aPKC enrichment on each side of the hair bundle confirmed that the ratio between the lateral bare zone and the medial side was significantly higher in mutants compared with controls (Fig. 3B). Of note, ectopic aPKC was previously reported upon *Gnai* and *Gpsm2* inactivation (Ezan et al., 2013; Tarchini et al., 2013), suggesting that aPKC invasion of the lateral apex in *Mpdz* mutants might be secondary to the downregulation of GNAI-GPSM2 there (Fig. 2). In contrast, aPKC was restricted medially at the cochlear apex at P4 (Fig. 3C) in *Mpdz* mutants, as in control HCs.

Together, our results demonstrate that MPDZ is essential to maintain, but not to initiate, properly polarized and segregated GNAI-GPSM2 and aPKC domains in maturing HCs after P4. Delocalized GNAI-GPSM2 enrichment at the flat HC surface and its corresponding loss at stereocilia tips likely contribute to disrupted stereocilia alignment and generally dysmorphic hair bundles (Fig. 1C,D). However, we do observe hair bundle defects at P0 already (Fig. 1C), suggesting that MPDZ impacts apical HC morphogenesis through other proteins as well.

MPDZ defines a Crumbs complex at the apical membrane in hair cells and choroid plexus cells

MPDZ was previously reported to localize and function at tight junctions in epithelial cells (Adachi et al., 2009; Hamazaki et al., 2002; Tetzlaff et al., 2018). Instead, our results revealed a role for MPDZ at the HC apical membrane, past the apical junction separating HCs from their support cell neighbors. MPDZ is a paralog of INADL (Adachi et al., 2009), a member of the CRB3-MPP5/PALS1-INADL Crumbs complex that is well known to regulate epithelial development and apico-basal polarization

Development (2021) 148, dev199549. doi:10.1242/dev.199549

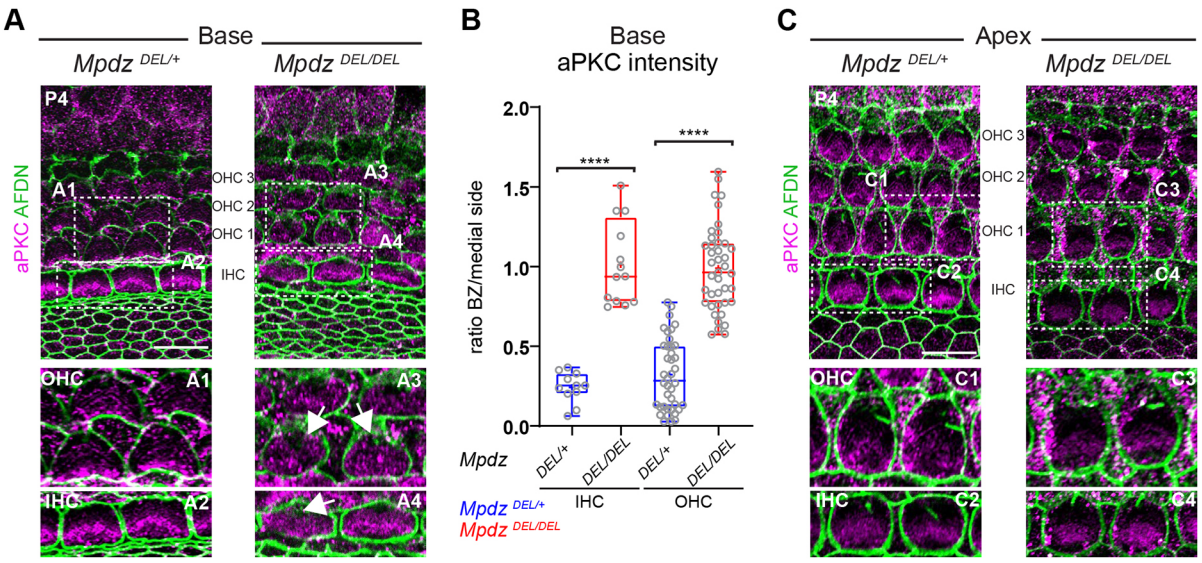

Fig. 3. aPKC medial restriction at the apical membrane is lost in the absence of MPDZ. (A-C) aPKC labeling (magenta) at P4 at the cochlear base (A) and apex (C). Apical junctions are labeled with afadin (AFDN; green). (A) The lateral bare zone, devoid of aPKC signal in controls, shows ectopic aPKC signal in *Mpdz* mutants in both OHCs and IHCs (arrows). (B) aPKC enrichment at the HC apical surface at the cochlear base. The ratio between signal intensity at the bare zone (BZ) and at the medial side is plotted. $Mpdz^{DEL/+}$ *N*=3, *n*=11 IHC, *n*=40 OHC; $Mpdz^{DEL/DEL}$ *N*=3, *n*=13 IHC, *n*=41 OHC (Mann–Whitney *U*-test; OHC and IHC: ****P<0.0001). (C) At the cochlear apex, aPKC is normally excluded from the bare zone in *Mpdz* mutants. The boxed regions (A1-A4; C1-C4) are magnified in the lower panels. Scale bars: 10 µm.

(Charrier et al., 2015; Roh et al., 2003; Straight et al., 2004; Whiteman et al., 2014). We next compared the localization of MPDZ and other Crumbs complex members in neonate HCs using ZO1 as marker for apical junctions, and surface (*xy*) and projection (*xz*) views of confocal stacks.

At P0 and P4, MPP5 was most highly enriched at the bare zone but also detected medially with little signal at the hair bundle (Fig. 4A), a distribution virtually identical to that of MPDZ (Fig. 1A). In addition, MPP5 was also detected at the HC apical junction (Fig. 4A, arrowheads). Projection views confirmed that MPP5, but not MPDZ, colocalized with ZO1 at OHC-support cell junctions (Fig. 4B, arrowheads). Occasional fixation artifacts separating the plasma membrane of HCs and neighboring support cells suggested that MPP5 was junctional in both cell types (Fig. S3A), as also expected from junctional MPP5 distribution at support cell-support cell contacts and outside the auditory epithelium (Fig. 4A). We next obtained a validated antibody raised against an intracellular epitope of CRB3 (Szymaniak et al., 2015). Although signal intensity was low, we observed CRB3 enrichment at the HC apical membrane and apical junctions, as for MPP5 (Fig. 4C). In contrast to the other members of the Crumbs complex, INADL was not detected at the HC apical membrane (Fig. S3B), and appeared instead limited to the apical junction of support cells (Fig. S3B,C). Together, these results suggest that a CRB3-MPP5-MPDZ complex occupies the HC apical membrane specifically.

Unlike CRB3-MPP5, MPDZ distribution in HCs did not include apical junctions, yet loss of MPDZ has been proposed to disrupt barrier integrity in ependymal and choroid plexus cells in part by compromising tight junctions (Feldner et al., 2017; Yang et al., 2019). To investigate this possible paradox, we immunolabeled MPDZ, CRB3 and MPP5 in the choroid plexus (4th ventricle) at P3 and P13-P15 in wild-type mice. Interestingly, we found that, as in the auditory epithelium, MPDZ was absent at ZO1-positive cell junctions in choroid plexus epithelial cells, but found at the apical membrane near the junctions (Fig. S4A,D,H). In contrast, MPP5 was clearly detected at apical junctions in addition to the apical membrane, as in HCs (Fig. S4B,E). CRB3 signal was low, but appeared to encompass the apical membrane at both stages, and the apical junctions at P13 (Fig. S4C,F). INADL was not detected at all (Fig. S4G). We conclude that in auditory and choroid plexus epithelial cells alike, CRB3-MPP5-MPDZ represents a Crumbs complex specifically addressed to the apical membrane. In both cell types, MPP5 and CRB3 also occupy the apical junctions, potentially with other partner(s).

MPDZ anchors MPP5 and CRB3 at the hair cell apex

MPDZ is expected to function as an anchor for partner proteins carrying a PDZ-binding domain, and MPDZ and MPP5 are known to interact directly (Adachi et al., 2009; Assemat et al., 2013). We wondered whether the loss of MPDZ would disrupt Crumbs complex partners in addition to GNAI-GPSM2 (Fig. 2) and aPKC (Fig. 3). At P0, MPP5 was missing at the bare zone in *Mpdz* mutants, and ectopically found in the hair bundle (Fig. 4D,E, filled arrowheads). Measuring MPP5 intensity ratio between the bare zone and the hair bundle confirmed this striking redistribution in *Mpdz* mutants (Fig. 4F). In contrast, MPP5 was still enriched at HC junctions in *Mpdz* mutants (Fig. 4D,E, unfilled arrowheads), in line with the lack of MPDZ at junctions (Fig. 4B). Measuring MPP5 junctional signal revealed a modest reduction in *Mpdz* mutants (Fig. 4G), however, suggesting that the distinct MPP5 complexes at the apical membrane and the junctions influence each other. Junctional integrity appeared grossly normal in *Mpdz* mutants, and in particular the precise intercalation of HCs and support cells in the auditory organ was unaffected (Fig. S5A). As with MPP5, we observed that CRB3 was lost at the bare zone and ectopically found in the hair bundle in P0 *Mpdz* mutants (Fig. S5B,C). As expected from its localization at support cell junctions, INADL was undetected in *Mpdz* mutant HCs (Fig. S5D).

As we observed disruption of MPP5 and CRB3 at an earlier stage (P0) than GNAI-GPSM2 and aPKC (P4) in *Mpdz* mutants, we

Development (2021) 148, dev199549. doi:10.1242/dev.199549

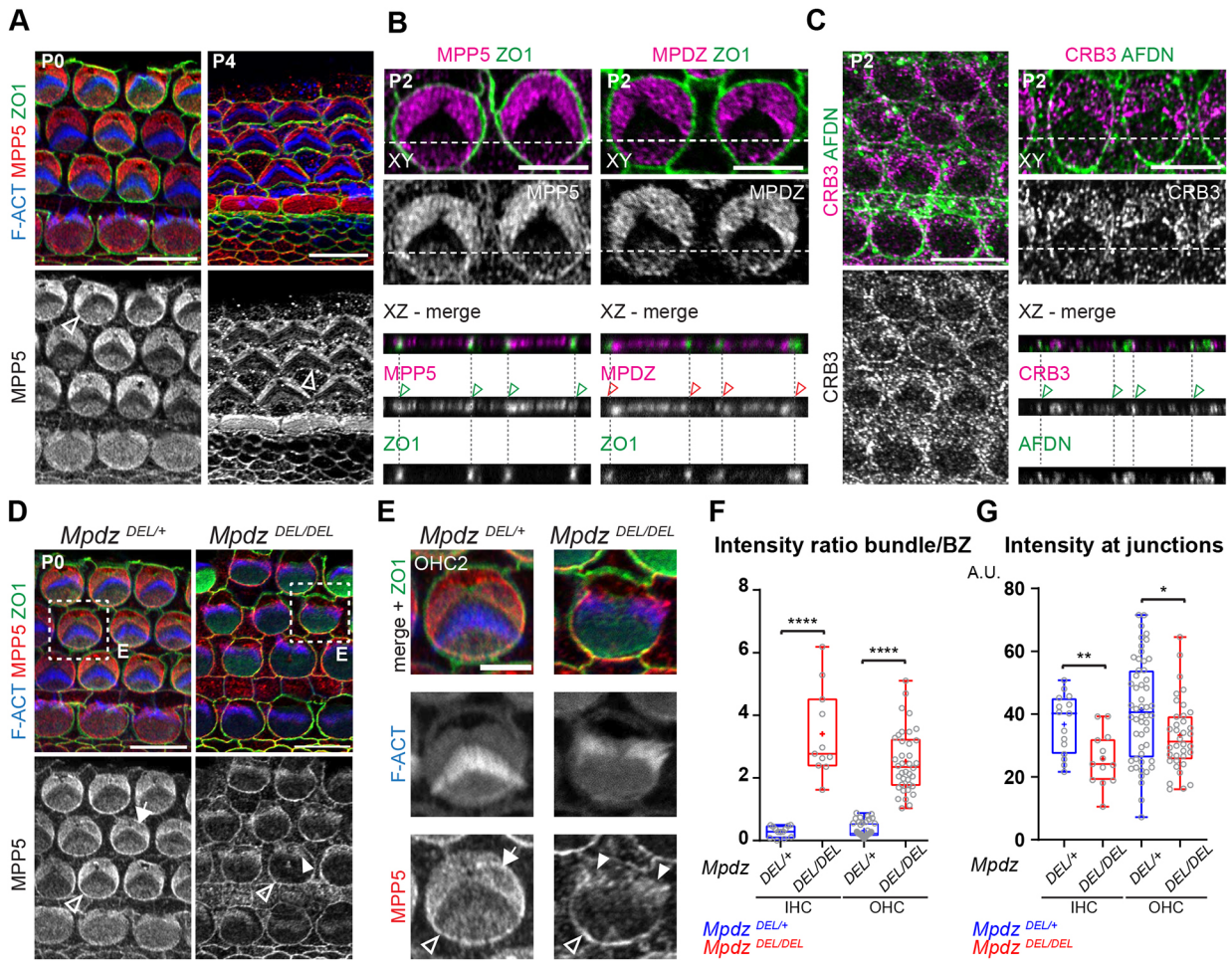

Fig. 4. MPDZ coincides with MPP5 and CRB3 and is required for their correct distribution at the hair cell apical membrane. (A-C) Immunolabeling in flat (*xy*) and projection (*xz*) views of the auditory epithelium between P0 and P4. (A) MPP5 immunolabeling reveals a similar protein distribution to MPDZ (see Fig. 1A). (B) A projection view also shows MPP5 co-enrichment with ZO1 at the HC-support cell junctions (green arrowheads). MPP5 is enriched at both the HC and support cell junction (see Fig. S3A). In contrast, MPDZ is not co-detected with ZO1 at apical junctions (red arrowheads). (C) CRB3 distribution is similar to that of MPP5 (A,B), encompassing both the apical membrane and the apical junctions (green arrowheads). AFDN was used to visualize apical junctions in C as ZO1 signal was compromised by the antigen retrieval procedure. (D,E) MPP5 labeling in P0 *Mpdz* mutant. In the absence of MPDZ, MPP5 is lost at the bare zone (arrow) and found ectopically in the hair bundle (filled arrowheads). MPP5 is retained at apical junctions (unfilled arrowheads). The boxed regions in D are magnified in E. (F,G) Apical MPP5 enrichment in P0 HCs at the cochlear base. The ratio between the MPP5 signals at the hair bundle and bare zone (F), and the MPP5 signal at the medial apical junction (G) are plotted. (F) $Mpdz^{DEL/+}$ *N*=3, *n*=13 IHC, *n*=49 OHC; $Mpdz^{DEL/DEL}$ *N*=3, *n*=11 IHC, *n*=38 OHC (Mann–Whitney *U*-test; IHC and OHC: ****P<0.0001). (G) $Mpdz^{DEL/+}$ *N*=3, *n*=15 IHC, *n*=52 OHC; $Mpdz^{DEL/DEL}$ *N*=3, *n*=13 IHC, *n*=36 OHC (Mann–Whitney *U*-test; IHC: **P=0.0044; OHC: *P=0.0175). Cochlear base (A,C left, D,E), cochlear mid (B,C right). A.U., arbitrary units. Scale bars: 10 µm (A,C left,D); 5 µm (B,C right,E).

conclude that MPDZ is directly required to anchor its Crumbs complex partners MPP5-CRB3 at the HC apical membrane. In turn, loss of the Crumbs complex at the flat apical membrane disrupts the polarization and segregation of GNAI-GPSM2 and aPKC. Hair bundle defects already observed at P0 (Fig. 1C,D) may be caused by abnormal localization of CRB3-MPP5 in stereocilia.

GNAI-GPSM2 and MPDZ-MPP5 influence each other at the hair cell apical membrane

MPDZ is required to maintain the lateral polarization of GNAI-GPSM2 at the apical membrane from P4 (Fig. 2), and CRB3-MPP5-MPDZ is more highly enriched at the bare zone compared with the medial HC surface (Figs 1A and 4A-C). We thus reasoned that, reciprocally, GNAI-GPSM2 might influence the distribution of MPDZ and MPP5. To test this prediction, we analyzed a constitutive *Gpsm2* mutant ($Gpsm2^{DEL}$) (Tarchini et al., 2013) and we globally downregulated GNAI activity in HCs by expressing the catalytic subunit of Pertussis toxin (PTXa) with *Atoh1-Cre* (Tarchini et al., 2016). At P4, *Gpsm2* mutant HCs lost their preferential MPDZ enrichment at the bare zone (Fig. 5A). Measuring the ratio of signal intensity on the medial versus lateral side of the hair bundle confirmed a more uniform MPDZ distribution across the apical surface upon loss of GPSM2 (Fig. 5B). Surprisingly, however, these quantifications also revealed that MPDZ signal intensity actually increased both on the medial and lateral sides in *Gpsm2* mutants, only more drastically on the medial side (Fig. 5C).

We also observed more uniform MPDZ distribution across the HC apex in PTXa-expressing HCs at P4 (Fig. 5D). Of note, PTXa provokes severe defects in OHC orientation (Kindt et al., 2021; Tarchini et al., 2013, 2016), and consequently the bare zone was no longer systematically on the lateral side of the auditory epithelium. We next immunolabeled MPP5 in *Gpsm2* and PTXa mutants because MPP5 binds (Adachi et al., 2009; Assemat et al., 2013) and colocalizes with MPDZ at the HC surface. As with MPDZ,

Development (2021) 148, dev199549. doi:10.1242/dev.199549

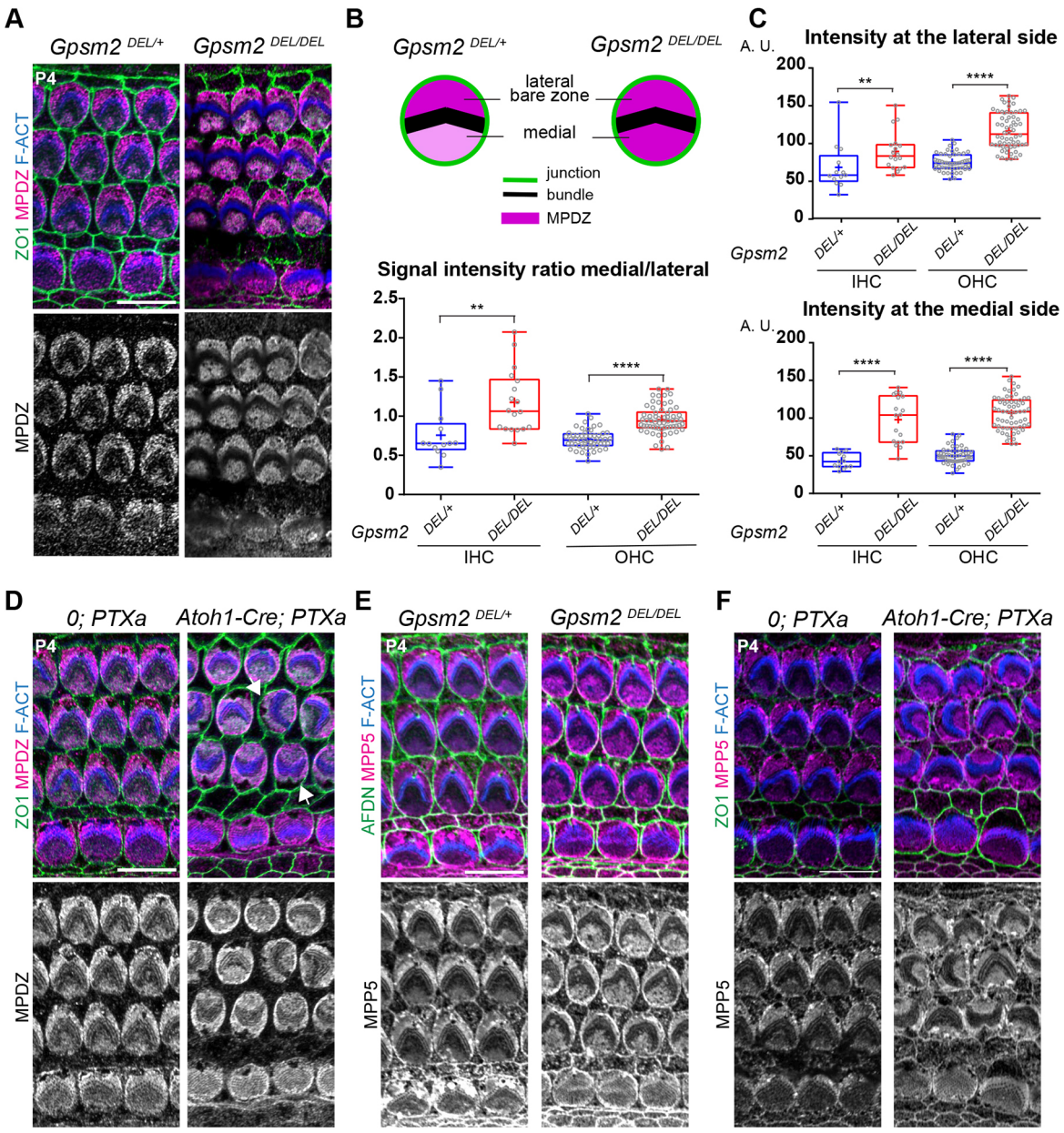

Fig. 5. GNAI-GPSM2 promotes planar polarization of MPDZ and MPP5 at the apical membrane. (A) MPDZ labeling (magenta) at P4 (cochlear apex). MPDZ lacks higher enrichment at the lateral bare zone in the absence of GPSM2. (B,C) MPDZ enrichment in HCs at P4 (cochlear apex). The ratio between the medial and lateral (bare zone) MPDZ signals (B), and the individual signals at the bare zone (C, top) and medial apex (C, bottom) are plotted. Note how MPDZ signals increase in both compartments in *Gpsm2* mutants, but more strongly at the medial apex. For all graphs: $Mpdz^{DEL/+}$ *N*=3, *n*=13 IHC, *n*=52 OHC; $Mpdz^{DEL/DEL}$ *N*=3, *n*=18 IHC, *n*=62 OHC (Mann–Whitney *U*-test; (B) IHC: ***P*=0.0014, OHC: *****P*<0.0001; (C) lateral IHC: ***P*=0.0064, lateral OHC: *****P*<0.0001; medial IHC and OHC: *****P*<0.0001). (D) MPDZ labeling (magenta) in Pertussis toxin (PTXa)-expressing HCs at P4 (cochlear apex). MPDZ lacks higher enrichment at the bare zone when GNAI is inactivated by PTXa. GNAI inactivation provokes graded OHCs misorientation so that the bare zone region (arrows) is not consistently lateral in PTXa OHCs. (E,F) MPP5 labeling (magenta) in $Gpsm^{DEL/DEL}$ (E) and PTXa (F) HCs at P4 (cochlear apex). Like MPDZ (A-D), MPP5 is more uniformly enriched across the apical membrane when GPSM2 or GNAI is inactivated. In E, afadin (AFDN) was used instead of ZO1 to label the apical junctions. Scale bars: 10 µm.

preferential MPP5 enrichment at the bare zone was abolished in *Gpsm2* (Fig. 5E) and PTXa (Fig. 5F) mutant HCs at P4. Finally, CRB3 enrichment at the HC apical membrane was severely reduced in *Gpsm2* mutants, and CRB3 lost its polarization towards the bare zone as well (Fig. S6). Together, our results suggest that reciprocal interactions between CRB3-MPP5-MPDZ and GNAI-GPSM2 ensure that proper amounts of each protein complex are maintained at the bare zone. Increased MPDZ enrichment on both sides of the hair bundle in the absence of GPSM2 may indicate that GNAI-GPSM2 somehow limits the total amount of MPDZ allowed to occupy the apical membrane.

Progressive loss of the apical blueprint coincides with severe hair bundle defects and hearing loss in mature hair cells

Early loss of GNAI and GPSM2 in postmitotic HCs leads to hair bundle disorganization, stereocilia stunting and profound hearing loss in young adults (Beer-Hammer et al., 2018; Mauriac et al.,

Development (2021) 148, dev199549. doi:10.1242/dev.199549

2017; Tadenev et al., 2019; Tarchini et al., 2016). Therefore, we investigated how loss of MPDZ that provokes a later disruption of GNAI-GPSM2 (Fig. 2) impacts the auditory organ near maturity. At P21, we did not observe OHC or IHC death along the cochlea in *Mpdz* mutants based on MYO6 immunolabeling (Fig. 6A). This verifies that delocalized GNAI-GPSM2 and aPKC starting at P4 (Figs 2, 3) is not an indirect consequence of HC degeneration, but a failure to actively maintain polarized protein distribution.

GNAI delocalization in *Mpdz* mutants progresses from the cochlear base to the apex along with HC differentiation (Fig. 2A). We immunolabeled GNAI at P15 to determine how this defect progresses beyond P7 (Fig. 2A). At the cochlear base, GNAI signal was visible at stereocilia tips in control OHCs, but largely absent in mutant OHCs (Fig. 6B). In contrast, GNAI could be observed at stereocilia tips in both control and mutant OHCs at the cochlear apex (Fig. 6B). We conclude that variable loss of GNAI at stereocilia tips in P4 OHCs (Fig. 2E) evolves into a complete loss with time, and that the GNAI delocalization wave never reaches the apex of the cochlea in *Mpdz* mutants. In P15 IHCs, GNAI signal at stereocilia tips was still largely visible at both the cochlear base and apex in *Mpdz* mutants (Fig. 6B). This suggests that the milder GNAI disruption observed at P4 in IHCs (Fig. 2E) does not evolve much by P15, or perhaps that GNAI trafficking to IHC tips is only delayed in *Mpdz* mutants.

To resolve the hair bundle structure better, we performed scanning electron microscopy (SEM) at P21. At the cochlear

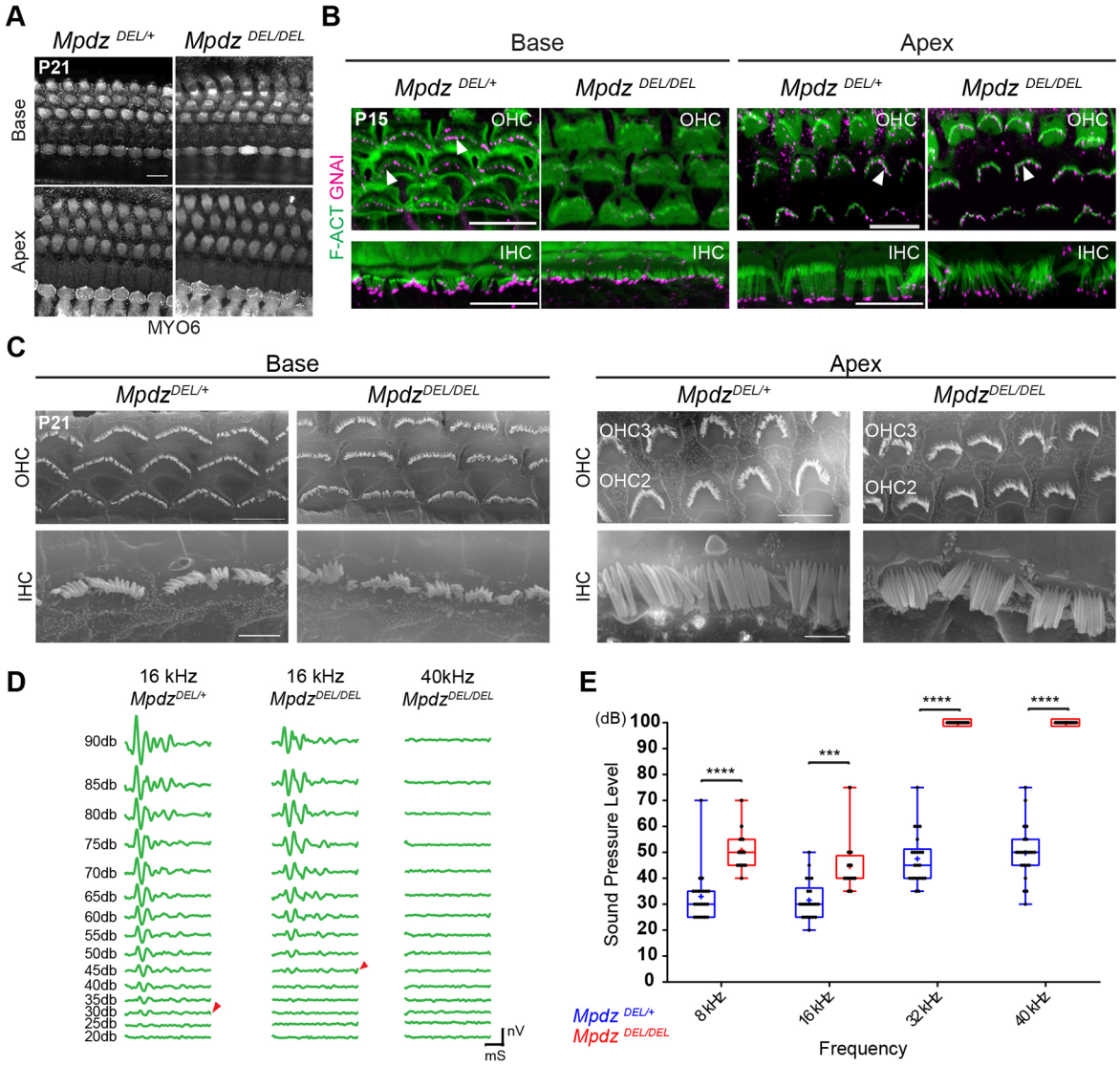

Fig. 6. Loss of MPDZ leads to tonotopically matching hair bundle and hearing defects in young adults. (A) MYO6 labeling of HCs at P21 (maximal projection). Despite severe apical patterning defects in neonates, no HC death is observed in young adults. (B) GNAI labeling (magenta) at P15 (maximal projection). GNAI signal at stereocilia tips (arrowheads) in control OHCs is lost in the *Mpdz* mutant at the cochlear base, but retained at the cochlear apex. In IHCs, GNAI signal is mostly retained at tips even at the cochlear base. (C) SEM images of representative OHCs and IHCs at P21 at the cochlear base and apex. Defects include flat and misshapen OHC bundles, and missing or irregular stereocilia placement in the first row in IHCs at the cochlear base. Hair bundle morphology in OHCs and IHCs is relatively normal at the cochlear apex. (D) ABR waveforms at variable sound pressure levels for one control littermate (16 kHz) and one *Mpdz* mutant (16 and 40 kHz). The threshold of ABR response is indicated (arrowheads). (E) ABR thresholds by genotype (8, 16, 32, 40 kHz). Animals of both sexes were tested between P21 and P25. $Mpdz^{DEL/+}$ N=22; $Mpdz^{DEL/DEL}$ N=12 (two-way ANOVA with Sidak's multiple comparison test; 8 kHz: ****P<0.0001; 16 kHz: ***P=0.0002; 32 kHz: ****P<0.0001; 40 kHz: ****P<0.0001). A plotted value of 100 dB indicates that animals did not respond at 90 dB. mS, millisecond; nV, nanovolt. Scale bars: 10 µm (A,B); 5 µm (C for OHCs); 2.5 µm (C for IHCs).

Development (2021) 148, dev199549. doi:10.1242/dev.199549

base, mutant OHCs retained a flattened hair bundle and a rounded apical circumference (Fig. 6C), as seen in neonates (Fig. 1C-G). Mutant IHCs were less affected but showed irregular stereocilia placement (Fig. 6C). At the cochlear apex, by contrast, OHC and IHC morphology was relatively normal, in line with normal localization of GNAI at the bare zone (P7; Fig. 2A) and stereocilia tips (P15; Fig. 6B).

To pair morphological alterations with organ function, we recorded auditory brainstem response (ABR) in 4-week-old *Mpdz* mutants and control littermates. We presented anesthetized animals with pure tone stimuli of variable sound pressure intensities (dB) to record ABR waveforms with a subcutaneous probe (Fig. 6D). Plotting ABR thresholds (Fig. 6D, arrowheads) by frequency and genotype revealed a severe hearing defect in *Mpdz* mutants (Fig. 6E). At high frequencies (32 and 40 kHz), *Mpdz* mutants showed complete hearing loss, with virtually no response to even the loudest stimuli (90 dB). At lower frequencies (8 and 16 kHz), *Mpdz* mutants did respond, but with a significantly higher threshold compared with control littermates. More severe hearing loss at higher frequencies was expected based on the tonotopic organization of HC frequency sensitivity along the cochlear duct: HCs at the cochlear apex, which are less affected in *Mpdz* mutants, detect lower frequencies.

DISCUSSION

We show that MPDZ is required to anchor a version of the Crumbs complex (CRB3-MPP5-MPDZ) at the HC apical membrane. Loss of MPDZ (and concomitant defects in MPP5-CRB3 apical enrichment) disrupts the maintenance of GNAI-GPSM2 and aPKC in their polarized and segregated apical domains (Fig. 7). Blurring of this molecular blueprint must contribute to stereocilia misalignment and dysmorphic hair bundles in *Mpdz* mutants, as similar defects were reported in the absence of GNAI or GPSM2. In turn, defective hair bundle morphogenesis is probably a leading cause for hearing loss in *Mpdz* mutants.

In the absence of MPDZ, hair bundle defects are visible at birth already, whereas defects in GNAI-GPSM2 and aPKC distribution are only noted from P4. Although delocalization of GNAI-GPSM2 is likely an important contributing factor, loss of MPDZ might interfere with other proteins required for early hair bundle development. Alternatively, relocalization of MPP5 and CRB3 from the flat HC apex to stereocilia at P0 (Fig. 4D,E; Fig. S5B,C) might cause hair bundle defects. CRB3 can interact with actin-binding proteins, including EPS8 (Gao et al., 2016) and ezrin (Whiteman et al., 2014). It is thus possible that ectopic MPP5-CRB3 presence in growing stereocilia interferes with F-actin assembly or its association with the plasma membrane, for example.

Progressive delocalization of GNAI-GPSM2 and aPKC at the HC apical membrane was previously reported in mutant HCs lacking the SMARCA4/BRG1 subunit of the SWI/SNF chromatin remodeling complex (Jin et al., 2016). Loss of SMARCA4 between P1 and P4 caused HCs to start dying from P8, however, possibly indicating that loss of protein polarization at the HC apical membrane is a side effect of cellular decline. In contrast to SMARCA4, loss of MPDZ does not lead to gross epithelial disorganization, and all HCs survive at least until P21. Maintaining the molecular blueprint that regulates cytoskeleton distribution at the HC surface is thus an active process. This conclusion is supported by another recent study in which disruption of proteostasis in postnatal HCs also affected the polarized distribution of blueprint proteins in the absence of HC death (Freeman et al., 2019).

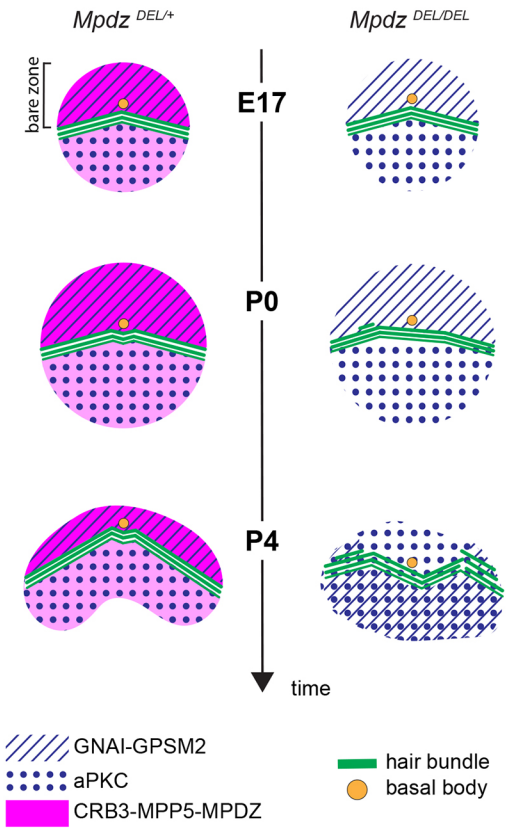

Fig. 7. Model of MPDZ function at the hair cell apical surface. Unlike GNAI-GPSM2 restricted to the bare zone (hatched), the Crumbs complex at the apical membrane (CRB3-MPP5-MPDZ, magenta) is also detected on the medial side of the hair bundle, although at lower levels. In the absence of MPDZ (and thus CRB3-MPP5), the GNAI-GPSM2 versus aPKC (dotted) blueprint is not maintained from P4, and stereocilia placement is defective.

Mpdz is one of only a few genes associated with congenital hydrocephalus, and two studies inactivating *Mpdz* in mouse reported severe hydrocephalus that proved lethal before or around 3 weeks of life (Feldner et al., 2017; Yang et al., 2019). The mouse models analyzed were a gene-trap allele in intron 11-12 in the C57BL/6J background (Feldner et al., 2017; Milner et al., 2015; Yang et al., 2019) and a conditional deletion of exons 4-5 in the C57BL/6 background (sub-strain unknown) (Feldner et al., 2017), both expected to produce a loss of function. Intriguingly, we do not observe hydrocephalus in $Mpdz^{DEL/DEL}$ mutants produced by the KOMP consortium (C57BL/6N-$Mpdz^{em1(IMPC)J}$/Mmucd), in which an indel in exon 6 is expected to truncate the protein after the first of 13 PDZ domains. Despite a sub-Mendelian frequency of homozygotes before weaning age, we could obtain and breed $Mpdz^{DEL/DEL}$ adults of both sexes (see Table S1 for a comparison between *Mpdz* alleles). We propose that this discrepancy stems from differences in genetic background between the C57BL6/J and C57BL6/N sub-strains (Simon et al., 2013). This is not necessarily surprising, as a study of another congenital hydrocephalus gene, *L1cam*, revealed a potent modifier locus on chromosome 5 (Tapanes-Castillo et al., 2010). In addition, there is precedent for one mutation to result in variable disease severity in these two sub-strains (Kang et al., 2019). Importantly, here we use a validated MPDZ antibody (Poliak et al., 2002) that showed a loss of signal in the choroid plexus of gene-trap *Mpdz* mutants (Yang et al., 2019), and shows a similar loss of signal in $Mpdz^{DEL/DEL}$ (Fig. S1A). Also considering the absence of signal in $Mpdz^{DEL/DEL}$ HCs (Fig. 1A),

Development (2021) 148, dev199549. doi:10.1242/dev.199549

we conclude that KOMP *Mpdz*^{DEL} is a bona fide loss-of-function allele. This is consistent with the severe morphological and auditory defects in *Mpdz*$^{DEL/DEL}$ mutants.

Interestingly, MPDZ is limited to the apical membrane in HCs and choroid plexus epithelial cells, and is not detected along with MPP5-CRB3 at apical junctions. Loss of MPDZ does, however, affect junctional integrity in the choroid plexus (Yang et al., 2019). It remains unclear whether defects in the remodeling of the HC circumference observed here are a secondary consequence of dysmorphic hair bundles, as shown previously in other mutants (Etournay et al., 2010), or whether MPDZ at the bare zone directly affects the contractility of neighboring junctions, for example. Interestingly, a recent report identified the Crumbs complex (CRB3-MPP5-INADL) as defining a transition zone between tight junctions and the free apical membrane, the 'vertebrate marginal zone' (Tan et al., 2020). Regardless of its mechanism, MPDZ acts as a positive regulator of junctional remodeling in HCs, and is notably required to limit the loss of apical surface area accompanying remodeling and to move away from a circular shape.

In contrast, MPDZ was reported to be enriched at apical junctions in other cell types (Adachi et al., 2009; Hamazaki et al., 2002; Marivin and Garcia-Marcos, 2019; Marivin et al., 2019; Tetzlaff et al., 2018). For example, the G protein regulator DAPLE and MPDZ colocalize and cooperate at junctions during apical cell constriction (Marivin and Garcia-Marcos, 2019; Marivin et al., 2019). As for *MPDZ*, *DAPLE* has been linked to congenital hydrocephalus in human and mice (Drielsma et al., 2012; Ekici et al., 2010; Takagishi et al., 2017). In auditory HCs, however, we showed that DAPLE is enriched laterally at the apical HC junction (Siletti et al., 2017), a distribution distinct from MPDZ at the HC apical membrane. In addition, apical HC defects in *Daple* mutants are more severe and distinct from those we report here in *Mpdz* mutants (Siletti et al., 2017). We thus conclude that MPDZ binding partners and MPDZ subcellular localization are dictated by the epithelial context.

The mechanism regulating the interplay between GNAI-GPSM2 and CRB3-MPP5-MPDZ remains unclear. GNAI-GPSM2 is strictly enriched laterally at the bare zone and appears to be required there to boost CRB3-MPP5-MPDZ levels compared with the medial side of the hair bundle (Fig. 7). Unexpectedly, however, GNAI-GPSM2 also limits overall MPDZ amounts at the apical membrane, as MPP5 and MPDZ are more evenly, but also more highly, enriched in the absence of GNAI-GPSM2. MPDZ might potentially bind to GNAI-GPSM2, and without anchorage at the bare zone, CRB3-MPP5-MPDZ might traffic there in excess and ultimately diffuse across the whole apex. Further work is needed to address these questions.

In summary, our results show that MPDZ specifically patterns the HC apical membrane, in part by maintaining the proper planar segregation of blueprint proteins at neonatal stages. Although we cannot rule out that the constitutive *Mpdz*^{DEL} mutation affects other cell types in the hearing pathway, loss of MPDZ leads to permanent hair bundle disorganization that is likely a major cause of severe hearing loss in young adults.

MATERIALS AND METHODS

Mice

The *Mpdz*^{DEL} strain (C57BL/6N-*Mpdz*$^{em1(IMPC)J}$/Mmucd, MGI: 5571597) was produced by the KOMP consortium at The Jackson Laboratory. *Gpsm2*^{DEL} (*Gpsm2*$^{tm1a(EUCOMM)Wtsi}$; MGI:4441912; Tarchini et al., 2013) and *R26-loxP-stop-loxP-mycPTXa* [*Gt (ROSA)26Sor*$^{em1(ptxA)Btar}$; MGI:6163665; Tarchini et al., 2016] were described previously. Wild-type samples analyzed were in a mixed genetic background (C57BL/6J×FVB/NJ). Mouse samples analyzed ranged in age from E17.5 to 4 weeks old, as indicated in each figure, and included both males and females. Heterozygote *Mpdz*$^{DEL/+}$ animals did not exhibit morphological, molecular or hearing defects, and were thus systematically used as littermate controls for *Mpdz*$^{DEL/DEL}$ mutants to reduce the number of animals produced for the study. Animals were maintained under standard housing and all animal work was reviewed for compliance and approved by the Animal Care and Use Committee of The Jackson Laboratory.

Immunofluorescence and antibodies

For embryonic and neonate stages, temporal bones were isolated and either immediately microdissected to expose the sensory epithelium before fixing in 4% paraformaldehyde (PFA) for 1 h at 4°C, or incubated in 10% trichloroacetic acid (TCA) for 10 min on ice before dissection, depending on the antibodies used (indicated below). After rinsing with PBS, the tectorial membrane was removed, and samples were blocked and permeabilized in PBS with 0.5% Triton X-100 and 1% bovine serum albumin for at least 1 h at room temperature before application of the primary antibodies. For CRB3 labeling, we used the following antigen retrieval procedure: the postnatal inner ear was fixed before microdissection for 1 h at room temperature in 4% PFA. The auditory epithelium was then exposed, blocked and permeabilized as described above for 20 min, and then incubated in 0.8 M urea for 1 h at 50°C, and then for 20 min at 65°C.

For postnatal stages after P7, temporal bones were isolated and the cochlea punctured at the apex to facilitate access of the fixative before immersion fixation in 4% PFA for 1 h at 4°C or room temperature. After rinsing with PBS, the temporal bone was incubated overnight at room temperature in 0.11 M EDTA for decalcification before dissection to expose the auditory epithelium. Samples were then blocked and permeabilized following the same protocol as for earlier stages.

The hindbrain (4th ventricle) choroid plexus was dissected at P3, P13 or P15, and fixed in 4% PFA for 1 h at 4°C. After rinsing with PBS, samples were blocked and permeabilized in PBS with 0.5% Triton X-100 and 1% bovine serum albumin for at least 1 h at room temperature before application of the primary antibodies.

Primary and secondary antibodies were each incubated overnight at 4°C in PBS. Fluorescent dye-conjugated phalloidin was added with the secondary antibodies. After each antibody incubation, samples were washed three times with PBS+0.05% Triton X-100 before a final post-fixation in 4% PFA for 1 h at room temperature. Samples were then mounted flat on a microscopy slide (Denville, M1021), either directly under a 18×18 mm #1.5 coverglass (VWR 48366-045) (cochlea), or using office tape as spacer (choroid plexus). Mowiol was used as mounting medium (Calbiochem/MilliporeSigma, 4759041). Mowiol (10% w/v) was prepared in 25% (w/v) glycerol and 0.1 M Tris-HCl, pH 8.5.

Primary antibodies used were: rabbit anti-MPDZ (Poliak et al., 2002) (gift from Elior Peles, Weizmann Institute of Science; PFA); rabbit anti-CRB3 (Szymaniak et al., 2015) (gift from Bob Varelas, Boston University; PFA); rabbit anti-TRIOBP/TARA (Proteintech, 16124-1-AP; PFA); rabbit anti-GNAI1/2/3 (Santa Cruz Biotechnology, sc-262; PFA; results in our laboratory indicate that this reagent is not specific for a single GNAI paralog and that at least GNAI2 and GNAI3 are colocalized apically in hair cells so we use 'GNAI' to refer to the signal obtained); rabbit anti-GPSM2 (Sigma-Aldrich, A41537; PFA); mouse anti-aPKC/PRKCZ (Santa Cruz Biotechnology, sc-216; PFA); sheep anti-AFDN/AF-6 (R&D Systems, AF7829; PFA); rat anti-ZO1 (Developmental Studies Hybridoma Bank, R26.4C; TCA or PFA); rabbit anti-MPP5 (Santa Cruz Biotechnology, sc-33831; PFA); rabbit anti-INADL (LifeSpan BioSciences, LS-C410011-50; TCA); rabbit anti-MYO6 (Proteus BioSciences, 25-6791; PFA); mouse anti-acetylated tubulin (Santa Cruz Biotechnology, 23950; PFA). Secondary antibodies were raised either in goat or donkey, and coupled to Alexa Fluor (AF) 488, 555 or 647 [Thermo Fisher Scientific, donkey anti-rabbit 488 (A-21206), 555 (A-31572), 647 (A-31573), donkey anti-mouse 555 (A-31570), 647 (A-31571), donkey anti-sheep 647 (A-21448), donkey anti-rat 488 (A-21208)]. We used fluorescence-conjugated phalloidins to reveal F-actin (Thermo Fisher Scientific, AF 488, A12379; Biotium, CF405, 89138-126).

Development (2021) 148, dev199549. doi:10.1242/dev.199549

FM 1-43 dye uptake

P4 inner ears were isolated in PBS and microdissected to expose the sensory epithelium. The lateral wall was removed and the sensory epithelium was carefully pulled off the modiolus and explanted in a drop of DMEM-F12 on a glass slide previously coated with poly-D-lysine (10 µg/ml). Explants were rinsed with 1× HBSS (no calcium or magnesium). Explants were then incubated in chilled FM 1-43 diluted in HBSS (final concentration 5 µM) for 10 s, and then rinsed six times in HBSS. Explants were then mounted in HBSS (with HEPES, calcium and magnesium) and imaged immediately.

Image acquisition and quantification

Images were captured using a LSM800 line scanning confocal microscope using Zen2.3 or Zen 2.6 software, an Airyscan detector in regular confocal mode, and a 63×1.4 NA oil objective lens (Carl Zeiss AG). FM 1-43 signals were captured using a DM5500B fluorescence microscope using the Leica Application Suite X (LAS X) and a 40× air objective (Leica). Unless stated otherwise in the figure legend, all images show a single optical plane. Images were processed using Adobe Photoshop (CC 2020), and the same image treatment was applied across genotypes or conditions in the same experiment. In all experiments, quantifications include at least three animals of each genotype. All experimental values plotted in the study, as well as animal cohort size and hair cell numbers are detailed in Table S2 where each tabulation reports on a single experiment. All animal (N) and cell (n) numbers analyzed are also indicated in the figure legends. Results in all three OHC rows were pooled because we did not observe a row-specific trend.

To measure hair cell apical surface area and the circularity of hair cells apical circumference (Fig. 1F,G), *z*-series stacks were acquired for each sample either at the base or the apex, and a single *z* slice was selected based on junctional ZO1 signal. The ZO1-positive outline of the hair cell was traced and the surface area and circularity measured using Fiji/ImageJ. The surface area is in μm^2 and the circularity is a value between 0 and 1, where 1 is a perfect circle. To measure immunolabeling signal intensity, microscopy fields were selected in which hair cells were mounted as flat as possible so as to avoid artifacts. *Z*-series stacks were acquired at the cochlear base using the same laser intensity and gain for all samples (mutant and control littermates), and a single *z* slice/optical plane was chosen in which the signal was the strongest. ZO1 or AFDN were used to label the apical hair cell junction, and the base of the stereocilia bundle (phalloidin) was used to distinguish the bare zone (lateral) and the medial sides of the apical membrane. Fiji/ImageJ was used to measure the mean gray value in a region of interest (ROI), as defined below. For each image, background signal was sampled and averaged, then subtracted from all hair cell quantifications on the same image.

To measure GNAI signal intensity in *Mpdz* mutants (Fig. 2D), the lateral (bare zone) and medial compartments were divided into three ROIs of equal width (a, b, c in the bare zone, d, e, f in the medial side, see Fig. 2D), and the mean gray value of each region was measured. To obtain the mean gray value of the entire bare zone and medial compartments (Fig. 2B), values in the three ROIs were averaged. To measure aPKC (Fig. 3B) and MPP5 (Fig. 4F) signals in *Mpdz* mutants, a fixed ROI was positioned that covered ∼50% of the apical compartments considered (bare zone, medial apex, hair bundle). To measure MPP5 intensity at junctions (Fig. 4G), a rectangular ROI of 0.15 μm^2 (1.5×0.1 µm) was positioned at the medial hair cell junction. To measure MPDZ intensity in *Gpsm2* mutants (Fig. 5B,C), a circular ROI of 1.054 μm^2 was positioned at the lateral (bare zone) and medial apical compartments.

SEM

Temporal bones were isolated from the skull, a hole was punctured at the cochlear apex, and samples were fixed by immersion at least overnight at 4°C in 2.5% glutaraldehyde+4% PFA (Electron Microscopy Science) in a 1 mM $MgCl_2$, 0.1 M sodium cacodylate, 20 mM $CaCl_2$ buffer. After rinses in PBS, samples were decalcified overnight with 0.11 M EDTA and the auditory epithelium was dissected into three pieces (cochlear base, mid, apex). Dissected samples were progressively dehydrated in an ethanol series (30-50-70-80-90-100%, for at least 20 min each). Chemical sample drying was carried out with hexamethyldisilazane (HMDS; Electron Microscopy Science, 50-243-18). Dry samples were then mounted onto aluminum stubs using double-sided carbon tape, and sputter-coated with gold-palladium before imaging on a Hitachi 3000N VP electron microscope. Images were taken at 20 kV and with a 5k magnification.

ABR tests

Mice were anesthetized by intraperitoneal injection of a mix of ketamine and xylazine (10 mg and 0.1 mg per 10 g of body weight, respectively) and body temperature was maintained at 37°C using a heating pad (FHC). All tests were conducted in a sound-attenuating chamber. ABR testing was performed using the RZ6 Multi-I/O Processor System coupled to the RA4PA 4-channel Medusa Amplifier (Tucker-Davis Technology; TDT system). Tone bursts at 8, 16, 32 and 40 kHz were generated with the TDT system, and sub-dermal needles were used as electrodes, with the active electrode inserted at the cranial vertex, the reference electrode under the left ear, and the ground electrode at the right thigh. Auditory thresholds were obtained for each stimulus by reducing the sound pressure level (SPL) by 5 dB steps between 90 and 20 dB to determine at which SPL an ABR could be recognized. $Mpdz^{DEL/DEL}$ mutants and $Mpdz^{DEL/+}$ control littermates were tested between ages P21 and P24. Both sexes were tested (see Table S2), and because sex had no influence on thresholds, sexes were pooled in Fig. 6E.

Statistical analysis

Data were plotted in Prism 8 (GraphPad). All values were plotted individually, and the distribution was framed with 25-75% whisker boxes where exterior lines show the minimum and maximum, the middle line representing the median, and a cross is used for the mean. A potential difference in data distribution between genotypes was tested for significance using the Mann–Whitney *U*-test (non-parametric unpaired *t*-test), except in the following cases: (1) GNAI signal intensity in lateral and medial apical compartments in control and *Mpdz* mutants (Fig. 2B), for which we used Kruskal–Wallis with a Dunn's multiple comparison test; (2) GNAI signal intensity by sub-region (Fig. 2D; Fig. S2), as well as ABR thresholds (Fig. 6D), for which we used two-way ANOVA with a Sidak's multiple comparison test. Exact *P*-values are indicated in the figure legends when calculated by Prism 8, and *P*-values are summarized on graphical plots by asterisks [****P<0.0001, ***P<0.001, **P<0.01, *P<0.05; P>0.05 considered not significant (ns)]. When not quantified, all immunolabeling experiments included at least three mutant samples in two litters, and a similar number of littermate control animals. In that case, figure panels show a representative outcome observed in all mutant samples.

Acknowledgements

We are very grateful to Dr Elior Peles (Weizmann Institute of Science) for sharing the MPDZ antibody, and to Dr Xaralabos Varelas (Boston University) for sharing the CRB3 antibody. The Mpdz mouse model was produced by the KOMP program led by Steve Murray at The Jackson Laboratory, and was shared by the group of Patsy Nishina.

Competing interests

The authors declare no competing or financial interests.

Author contributions

Conceptualization: B.T.; Validation: A.J.; Formal analysis: A.J.; Investigation: A.J.; Resources: B.T.; Data curation: A.J.; Writing - original draft: A.J., B.T.; Writing - review & editing: A.J., B.T.; Visualization: A.J.; Supervision: B.T.; Project administration: B.T.; Funding acquisition: B.T.

Funding

A.J. was supported by a 2-year postdoctoral fellowship from Fondation pour l'Audition (FPA RD2018-3). This work was supported by the National Institute on Deafness and Other Communication Disorders (R01 DC015242 and DC018304 to B.T.). Deposited in PMC for release after 12 months.

Peer review history

The peer review history is available online at https://journals.biologists.com/dev/article-lookup/doi/10.1242/dev.199549

References

Adachi, M., Hamazaki, Y., Kobayashi, Y., Itoh, M., Tsukita, S., Furuse, M. and Tsukita, S. (2009). Similar and distinct properties of MUPP1 and Patj, two homologous PDZ domain-containing tight-junction proteins. *Mol. Cell. Biol.* **29**, 2372-2389. doi:10.1128/MCB.01505-08

Al-Dosari, M., Al-Owain, M., Tulbah, M., Kurdi, W., Adly, N., Al-Hemidan, A., Masoodi, T., Albash, B. and FS, A. (2013). Mutation in MPDZ causes severe congenital hydrocephalus. *J. Med. Genet.* **50**, 54-58. doi:10.1136/jmedgenet-2012-101294

Al-Jezawi, N. K., Al-Shamsi, A. M., Suleiman, N., Ben-Salem, S., John, A., Vijayan, R., Ali, B. R. and Al-Gazali, L. (2018). Compound heterozygous variants in the multiple PDZ domain protein (MPDZ) cause a case of mild non-progressive communicating hydrocephalus. *BMC Med. Genet.* **19**, 1-11. doi:10.1186/s12881-018-0540-x

Assémat, E., Bazellières, E., Pallesi-Pocachard, E., Le Bivic, A. and Massey-Harroche, D. (2008). Polarity complex proteins. *Biochim. Biophys. Acta* **1778**, 614-630. doi:10.1016/j.bbamem.2007.08.029

Assemat, E., Crost, E., Ponserre, M., Wijnholds, J., Le Bivic, A. and Massey-Harroche, D. (2013). The multi-PDZ domain protein-1 (MUPP-1) expression regulates cellular levels of the PALS-1/PATJ polarity complex. *Exp. Cell Res.* **319**, 2514-2525. doi:10.1016/j.yexcr.2013.07.011

Barr-Gillespie, P. G. (2015). Assembly of hair bundles, an amazing problem for cell biology. *Mol. Biol. Cell* **26**, 2727-2732. doi:10.1091/mbc.E14-04-0940

Beer-Hammer, S., Lee, S. C., Mauriac, S. A., Leiss, V., Groh, I. A. M., Novakovic, A., Piekorz, R. P., Bucher, K., Chen, C., Ni, K. et al. (2018). Galphai proteins are indispensable for hearing. *Cell. Physiol. Biochem.* **47**, 1509-1532. doi:10.1159/000490867

Bhonker, Y., Abu-Rayyan, A., Ushakov, K., Amir-Zilberstein, L., Shivatzki, S., Yizhar-Barnea, O., Elkan-Miller, T., Tayeb-Fligelman, E., Kim, S. M., Landau, M. et al. (2016). The GPSM2/LGN GoLoco motifs are essential for hearing. *Mamm. Genome* **27**, 29-46. doi:10.1007/s00335-015-9614-7

Charrier, L. E., Loie, E. and Laprise, P. (2015). Mouse Crumbs3 sustains epithelial tissue morphogenesis in vivo. *Sci. Rep.* **5**, 17699. doi:10.1038/srep17699

Deans, M. R. (2013). A balance of form and function: planar polarity and development of the vestibular maculae. *Semin. Cell Dev. Biol.* **24**, 490-498. doi:10.1016/j.semcdb.2013.03.001

Doherty, D., Chudley, A. E., Coghlan, G., Ishak, G. E., Innes, A. M., Lemire, E. G., Rogers, R. C., Mhanni, A. A., Phelps, I. G., Jones, S. J. et al. (2012). GPSM2 mutations cause the brain malformations and hearing loss in Chudley-McCullough syndrome. *Am. J. Hum. Genet.* **90**, 1088-1093. doi:10.1016/j.ajhg.2012.04.008

Drielsma, A., Jalas, C., Simonis, N., Desir, J., Simanovsky, N., Pirson, I., Elpeleg, O., Abramowicz, M. and Edvardson, S. (2012). Two novel CCDC88C mutations confirm the role of DAPLE in autosomal recessive congenital hydrocephalus. *J. Med. Genet.* **49**, 708-712. doi:10.1136/jmedgenet-2012-101190

Ekici, A. B., Hilfinger, D., Jatzwauk, M., Thiel, C. T., Wenzel, D., Lorenz, I., Boltshauser, E., Goecke, T. W., Staatz, G., Morris-Rosendahl, D. J. et al. (2010). Disturbed Wnt signalling due to a mutation in CCDC88C causes an autosomal recessive non-syndromic hydrocephalus with medial diverticulum. *Mol. Syndromol.* **1**, 99-112. doi:10.1159/000319859

Etournay, R., Lepelletier, L., Boutet de Monvel, J., Michel, V., Cayet, N., Leibovici, M., Weil, D., Foucher, I., Hardelin, J. P. and Petit, C. (2010). Cochlear outer hair cells undergo an apical circumference remodeling constrained by the hair bundle shape. *Development* **137**, 1373-1383. doi:10.1242/dev.045138

Ezan, J., Lasvaux, L., Gezer, A., Novakovic, A., May-Simera, H., Belotti, E., Lhoumeau, A. C., Birnbaumer, L., Beer-Hammer, S., Borg, J. P. et al. (2013). Primary cilium migration depends on G-protein signalling control of subapical cytoskeleton. *Nat. Cell Biol.* **15**, 1107-1115. doi:10.1038/ncb2819

Feldner, A., Adam, M. G., Tetzlaff, F., Moll, I., Komljenovic, D., Sahm, F., Bauerle, T., Ishikawa, H., Schroten, H., Korff, T. et al. (2017). Loss of Mpdz impairs ependymal cell integrity leading to perinatal-onset hydrocephalus in mice. *EMBO Mol. Med.* **9**, 890-905. doi:10.15252/emmm.201606430

Freeman, S., Mateo Sanchez, S., Pouyo, R., Van Lerberghe, P. B., Hanon, K., Thelen, N., Thiry, M., Morelli, G., Van Hees, L., Laguesse, S. et al. (2019). Proteostasis is essential during cochlear development for neuron survival and hair cell polarity. *EMBO Rep.* **20**, e47097. doi:10.15252/embr.201847097

Gao, Y., Lui, W., Lee, W. and Cheng, C. (2016). Polarity protein Crumbs homolog-3 (CRB3) regulates ectoplasmic specialization dynamics through its action on F-actin organization in Sertoli cells. *Sci. Rep.* **6**, 28589. doi:10.1038/srep28589

Hamazaki, Y., Itoh, M., Sasaki, H., Furuse, M. and Tsukita, S. (2002). Multi-PDZ domain protein 1 (MUPP1) is concentrated at tight junctions through its possible interaction with claudin-1 and junctional adhesion molecule. *J. Biol. Chem.* **277**, 455-461. doi:10.1074/jbc.M109005200

Hurd, T. W., Gao, L., Roh, M. H., Macara, I. G. and Margolis, B. (2003). Direct interaction of two polarity complexes implicated in epithelial tight junction assembly. *Nat. Cell Biol.* **5**, 137-142. doi:10.1038/ncb923

Jin, Y., Ren, N., Li, S., Fu, X., Sun, X., Men, Y., Xu, Z., Zhang, J., Xie, Y., Xia, M. et al. (2016). Deletion of Brg1 causes abnormal hair cell planer polarity, hair cell anchorage, and scar formation in mouse cochlea. *Sci. Rep.* **6**, 1-14. doi:10.1038/s41598-016-0001-8

Kang, S. K., Hawkins, N. A. and Kearney, J. A. (2019). C57BL/6J and C57BL/6N substrains differentially influence phenotype severity in the Scn1a (+/-) mouse model of Dravet syndrome. *Epilepsia Open* **4**, 164-169. doi:10.1002/epi4.12287

Katsuno, T., Belyantseva, I. A., Cartagena-Rivera, A. X., Ohta, K., Crump, S. M., Petralia, R. S., Ono, K., Tona, R., Imtiaz, A., Rehman, A. et al. (2019). TRIOBP-5 sculpts stereocilia rootlets and stiffens supporting cells enabling hearing. *JCI Insight* **4**, e128561. doi:10.1172/jci.insight.128561

Kindt, K. S., Akturk, A., Jarysta, A., Day, M., Beirl, A., Flonard, M. and Tarchini, B. (2021). EMX2-GPR156-Galphai reverses hair cell orientation in mechanosensory epithelia. *Nat. Commun.* **12**, 2861. doi:10.1038/s41467-021-22997-1

Krapivinsky, G., Medina, I., Krapivinsky, L., Gapon, S. and Clapham, D. (2004). SynGAP-MUPP1-CaMKII synaptic complexes regulate p38 MAP kinase activity and NMDA receptor-dependent synaptic AMPA receptor potentiation. *Neuron* **43**, 563-574. doi:10.1016/j.neuron.2004.08.003

Lanaspa, M. A., Andres-Hernando, A., Rivard, C. J., Dai, Y. and Berl, T. (2008). Hypertonic stress increases claudin-4 expression and tight junction integrity in association with MUPP1 in IMCD3 cells. *Proc. Natl. Aacd. Sci. USA* **105**, 15797-15802. doi:10.1073/pnas.0805761105

Landin Malt, A., Dailey, Z., Holbrook-Rasmussen, J., Zheng, Y., Hogan, A., Du, Q. and Lu, X. (2019). Par3 is essential for the establishment of planar cell polarity of inner ear hair cells. *Proc. Natl. Aacd. Sci. USA* **116**, 4999-5008. doi:10.1073/pnas.1816333116

Landin Malt, A., Hogan, A. K., Smith, C. D., Madani, M. S. and Lu, X. (2020). Wnts regulate planar cell polarity via heterotrimeric G protein and PI3K signaling. *J. Cell Biol.* **219**, e201912071. doi:10.1083/jcb.201912071

Lemmers, C., Medina, E., Delgrossi, M. H., Michel, D., Arsanto, J. P. and Le Bivic, A. (2002). hINADl/PATJ, a homolog of discs lost, interacts with crumbs and localizes to tight junctions in human epithelial cells. *J. Biol. Chem.* **277**, 25408-25415. doi:10.1074/jbc.M202196200

Makarova, O., Roh, M. H., Liu, C. J., Laurinec, S. and Margolis, B. (2003). Mammalian Crumbs3 is a small transmembrane protein linked to protein associated with Lin-7 (Pals1). *Gene* **302**, 21-29. doi:10.1016/S0378111902010843

Marivin, A. and Garcia-Marcos, M. (2019). DAPLE and MPDZ bind to each other and cooperate to promote apical cell constriction. *Mol. Biol. Cell* **30**, 1900-1910. doi:10.1091/mbc.E19-02-0091

Marivin, A., Morozova, V., Walawalkar, I., Leyme, A., Kretov, D. A., Cifuentes, D., Dominguez, I. and Garcia-Marcos, M. (2019). GPCR-independent activation of G proteins promotes apical cell constriction in vivo. *J. Cell Biol.* **218**, 1743-1763. doi:10.1083/jcb.201811174

Mauriac, S. A., Hien, Y. E., Bird, J. E., Carvalho, S. D., Peyroutou, R., Lee, S. C., Moreau, M. M., Blanc, J. M., Geyser, A., Medina, C. et al. (2017). Defective Gpsm2/Galphai3 signalling disrupts stereocilia development and growth cone actin dynamics in Chudley-McCullough syndrome. *Nat. Commun.* **8**, 14907. doi:10.1038/ncomms14907

McGrath, J., Roy, P. and Perrin, B. J. (2017). Stereocilia morphogenesis and maintenance through regulation of actin stability. *Semin. Cell Dev. Biol.* **65**, 88-95. doi:10.1016/j.semcdb.2016.08.017

McKenzie, E., Krupin, A. and Kelley, M. W. (2004). Cellular growth and rearrangement during the development of the mammalian organ of Corti. *Dev. Dyn.* **229**, 802-812. doi:10.1002/dvdy.10500

Milner, L. C., Shirley, R. L., Kozell, L. B., Walter, N. A., Kruse, L. C., Komiyama, N. H., Grant, S. G. and Buck, K. J. (2015). Novel MPDZ/MUPP1 transgenic and knockdown models confirm Mpdz's role in ethanol withdrawal and support its role in voluntary ethanol consumption. *Addict. Biol.* **20**, 143-147. doi:10.1111/adb.12087

Najarro, E. H., Huang, J., Jacobo, A., Quiruz, L. A., Grillet, N. and Cheng, A. G. (2020). Dual regulation of planar polarization by secreted Wnts and Vangl2 in the developing mouse cochlea. *Development* **147**, dev191981.

Petit, C. and Richardson, G. P. (2009). Linking genes underlying deafness to hair-bundle development and function. *Nat. Neurosci.* **12**, 703-710. doi:10.1038/nn.2330

Poliak, S., Matlis, S., Ullmer, C., Scherer, S. S. and Peles, E. (2002). Distinct claudins and associated PDZ proteins form different autotypic tight junctions in myelinating Schwann cells. *J. Cell Biol.* **159**, 361-372. doi:10.1083/jcb.200207050

Roh, M. H., Fan, S., Liu, C. J. and Margolis, B. (2003). The Crumbs3-Pals1 complex participates in the establishment of polarity in mammalian epithelial cells. *J. Cell Sci.* **116**, 2895-2906. doi:10.1242/jcs.00500

Roh, M. H., Makarova, O., Liu, C. J., Shin, K., Lee, S., Laurinec, S., Goyal, M., Wiggins, R. and Margolis, B. (2002). The Maguk protein, Pals1, functions as an adapter, linking mammalian homologues of crumbs and discs lost. *J. Cell Biol.* **157**, 161-172. doi:10.1083/jcb.200109010

Saugier-Veber, P., Marguet, F., Lecoquierre, F., Adle-Biassette, H., Guimiot, F., Cipriani, S., Patrier, S., Brasseur-Daudruy, M., Goldenberg, A., Layet, V. et al. (2017). Hydrocephalus due to multiple ependymal malformations is caused by mutations in the MPDZ gene. *Acta Neuropathol Commun* **5**, 36. doi:10.1186/s40478-017-0438-4

Shaheen, R., Sebai, M., Patel, N., Ewida, N., Kurdi, W., Altweijri, I., Sogaty, S., Almardawi, E., Seidahmed, M., Alnemri, A. et al. (2017). The genetic landscape of familial congenital hydrocephalus. *Ann. Neurol.* **81**, 890-897. doi:10.1002/ana.24964

Shin, K., Straight, S. and Margolis, B. (2005). PATJ regulates tight junction formation and polarity in mammalian epithelial cells. *J. Cell Biol.* **168**, 705-711. doi:10.1083/jcb.200408064

Siletti, K., Tarchini, B. and Hudspeth, A. J. (2017). Daple coordinates organ-wide and cell-intrinsic polarity to pattern inner-ear hair bundles. *Proc. Natl. Aacd. Sci. USA* **114**, E11170-E11179. doi:10.1073/pnas.1716522115

Simon, M. M., Greenaway, S., White, J. K., Fuchs, H., Gailus-Durner, V., Wells, S., Sorg, T., Wong, K., Bedu, E., Cartwright, E. J. et al. (2013). A comparative phenotypic and genomic analysis of C57BL/6J and C57BL/6N mouse strains. *Genome Biol.* **14**, R82. doi:10.1186/gb-2013-14-7-r82

Simpson, E., Suffolk, R. and Jackson, I. (1999). Identification, sequence, and mapping of the mouse multiple PDZ domain protein gene, Mpdz. *Genomics* **59**, 102-104. doi:10.1006/geno.1999.5853

Straight, S. W., Shin, K., Fogg, V. C., Fan, S., Liu, C. J., Roh, M. and Margolis, B. (2004). Loss of PALS1 expression leads to tight junction and polarity defects. *Mol. Biol. Cell* **15**, 1981-1990. doi:10.1091/mbc.e03-08-0620

Szymaniak, A. D., Mahoney, J. E., Cardoso, W. V. and Varelas, X. (2015). Crumbs3-mediated polarity directs airway epithelial cell fate through the hippo pathway effector yap. *Dev. Cell* **34**, 283-296. doi:10.1016/j.devcel.2015.06.020

Tadenev, A. L. D., Akturk, A., Devanney, N., Mathur, P. D., Clark, A. M., Yang, J. and Tarchini, B. (2019). GPSM2-GNAI specifies the tallest stereocilia and defines hair bundle row identity. *Curr. Biol.* **29**, 921-934.e924. doi:10.1016/j.cub.2019.01.051

Takagishi, M., Sawada, M., Ohata, S., Asai, N., Enomoto, A., Takahashi, K., Weng, L., Ushida, K., Ara, H., Matsui, S. et al. (2017). Daple coordinates planar polarized microtubule dynamics in ependymal cells and contributes to hydrocephalus. *Cell Reports* **20**, 960-972. doi:10.1016/j.celrep.2017.06.089

Tan, B., Yatim, S., Peng, S., Gunaratne, J., Hunziker, W. and Ludwig, A. (2020). The mammalian crumbs complex defines a distinct polarity domain apical of epithelial tight junctions. *Curr. Biol.* **30**, 2791-2804.e2796. doi:10.1016/j.cub.2020.05.032

Tapanes-Castillo, A., Weaver, E., Smith, R., Kamei, Y., Caspary, T., Hamilton-Nelson, K., Slifer, S., Martin, E., Bixby, J. and Lemmon, V. (2010). A modifier locus on chromosome 5 contributes to L1 cell adhesion molecule X-linked hydrocephalus in mice. *Neurogenetics* **11**, 53-71. doi:10.1007/s10048-009-0203-3

Tarchini, B. and Lu, X. (2019). New insights into regulation and function of planar polarity in the inner ear. *Neurosci. Lett.* **709**, 134373. doi:10.1016/j.neulet.2019.134373

Tarchini, B., Jolicoeur, C. and Cayouette, M. (2013). A molecular blueprint at the apical surface establishes planar asymmetry in cochlear hair cells. *Dev. Cell* **27**, 88-102. doi:10.1016/j.devcel.2013.09.011

Tarchini, B., Tadenev, A. L., Devanney, N. and Cayouette, M. (2016). A link between planar polarity and staircase-like bundle architecture in hair cells. *Development* **143**, 3926-3932. doi:10.1242/dev.139089

Tepass, U. (2012). The apical polarity protein network in Drosophila epithelial cells: regulation of polarity, junctions, morphogenesis, cell growth, and survival. *Annu. Rev. Cell Dev. Biol.* **28**, 655-685. doi:10.1146/annurev-cellbio-092910-154033

Tetzlaff, F., Adam, M. G., Feldner, A., Moll, I., Menuchin, A., Rodriguez-Vita, J., Sprinzak, D. and Fischer, A. (2018). MPDZ promotes DLL4-induced Notch signaling during angiogenesis. *eLife* **7**, e32860. doi:10.7554/eLife.32860

Ullmer, C., Schmuck, K., Figge, A. and Lübbert, H. (1998). Cloning and characterization of MUPP1, a novel PDZ domain protein. *FEBS Lett.* **424**, 63-68. doi:10.1016/S0014-5793(98)00141-0

Velez-Ortega, A. C. and Frolenkov, G. I. (2019). Building and repairing the stereocilia cytoskeleton in mammalian auditory hair cells. *Hear. Res.* **376**, 47-57. doi:10.1016/j.heares.2018.12.012

Walsh, T., Shahin, H., Elkan-Miller, T., Lee, M. K., Thornton, A. M., Roeb, W., Abu Rayyan, A., Loulus, S., Avraham, K. B., King, M. C. et al. (2010). Whole exome sequencing and homozygosity mapping identify mutation in the cell polarity protein GPSM2 as the cause of nonsyndromic hearing loss DFNB82. *Am. J. Hum. Genet.* **87**, 90-94. doi:10.1016/j.ajhg.2010.05.010

Whiteman, E. L., Fan, S., Harder, J. L., Walton, K. D., Liu, C. J., Soofi, A., Fogg, V. C., Hershenson, M. B., Dressler, G. R., Deutsch, G. H. et al. (2014). Crumbs3 is essential for proper epithelial development and viability. *Mol. Cell. Biol.* **34**, 43-56. doi:10.1128/MCB.00999-13

Yang, J., Simonneau, C., Kilker, R., Oakley, L., Byrne, M. D., Nichtova, Z., Stefanescu, I., Pardeep-Kumar, F., Tripathi, S., Londin, E. et al. (2019). Murine MPDZ-linked hydrocephalus is caused by hyperpermeability of the choroid plexus. *EMBO Mol. Med.* **11**, e9540. doi:10.15252/emmm.201809540